UNIVERSITÀ
DI PARMA

Conferimento del titolo di
Dottore Magistrale ad honorem in
Chimica e Tecnologia Farmaceutiche *a*
William Allen Eaton

The Biophysical Basis of Drug Therapy for Sickle Cell Disease

Lectio doctoralis di

William Allen Eaton

Parma, Aula Magna

25 maggio 2018

Abstract

This thesis is concerned with exploiting our knowledge of the thermodynamics and kinetics of sickle cell hemoglobin polymerization to provide a quantitative rationale for developing sensitive and a patho-physiologically relevant assay to screen compounds to discover drugs for treating sickle cell disease. Chapter I presents the essential basic information about the disease, with some brief historical background. Chapter II describes how oxygen controls the thermodynamics of polymerization and shows that were polymerization at equilibrium, patients would not survive beyond 6 months after birth when fetal hemoglobin has been almost completely replaced by adult hemoglobin. The thermodynamic analysis also shows that both sickle cell trait, the heterozygous condition, and the compound heterozygous condition of sickle cell with pancellular hereditary persistence of fetal hemoglobin would both be clinically severe conditions were polymerization at equilibrium. Chapter III presents calculations of the kinetics of sickling under *in vivo* conditions of deoxygenation to partial pressures in the tissues. The calculations are validated by reproducing the results of the pioneering experiments on sickling of cells in which the carbon monoxide complex of sickle hemoglobin is partially or completely dissociated with a laser. The conclusion from these calculations is that the sickle cell disease is survivable because the vast majority of cells escape the narrow vessels of the tissues before formation of the sickle fibers that cause vaso-occlusion. These results indicate that it is not necessary to completely inhibit fiber formation to treat the disease. Amelioration should result by increasing the delay time of fiber formation to allow more cells to escape the microcirculation of the tissues before sickling occurs. Chapter IV presents the biophysical basis for five separate approaches to increasing the delay time that would be therapeutic. Chapter V describes a sensitive kinetic assay, which shows that a small increase in red cell

volume to decrease the intracellular hemoglobin concentration, taking advantage of the enormous concentration dependence of the delay time, should be therapeutic.

Le basi biofisiche della terapia farmacologica per l'anemia falciforme

Questa tesi spiega come le conoscenze di termodinamica e cinetica della reazione di polimerizzazione di emoglobina S in pazienti affetti da anemia falciforme forniscano le basi per un approccio quantitativo nello sviluppo di un saggio sensibile per lo screening di composti ad azione terapeutica.

Il capitolo I fornisce le informazioni essenziali sulla malattia con qualche breve accenno storico. Il capitolo II descrive come la concentrazione di ossigeno controlli la termodinamica della polimerizzazione, e dimostra che se il processo di polimerizzazione fosse all'equilibrio, i pazienti non sopravvivrebbero oltre sei mesi dopo la nascita quando l'emoglobina fetale viene completamente sostituita dall'emoglobina adulta. L'analisi termodinamica mostra anche che sia i pazienti eterozigoti per l'emoglobina S che quelli con una persistenza ereditaria di emoglobina fetale sarebbero in condizioni cliniche severe se la reazione di polimerizzazione dell'emoglobina S raggiungesse l'equilibrio. Il capitolo III presenta calcoli relativi alla cinetica di deformazione dei globuli rossi in condizioni di parziale deossigenazione nei tessuti *in vivo*. I calcoli sono confermati in quanto riproducono i risultati ottenuti in esperimenti di deformazione dei globuli rossi causata dal distacco parziale o completo dell'ossido di carbonio legato all'emoglobina S mediante fotolisi laser. La conclusione derivante da questi calcoli è che si può sopravvivere all'anemia falciforme perché la maggior parte dei globuli rossi passano attraverso gli stretti vasi della

microcircolazione prima che le fibre di emoglobina S, che causano la distorsione dei globuli rossi, la perdita di plasticità e quindi la vaso-occlusione, si formino. Questi risultati indicano che non è necessario inibire completamente la formazione delle fibre per curare la malattia. Un beneficio terapeutico potrebbe derivare da un allungamento del tempo di ritardo con cui si formano le fibre per permettere a più globuli rossi di passare attraverso la microcircolazione dei tessuti prima che ne avvenga la distorsione. Il capitolo IV presenta le basi biofisiche e biochimiche per cinque diversi approcci per aumentare il tempo di ritardo che potrebbero avere un effetto terapeutico. Il capitolo V descrive un saggio cinetico estremamente sensibile che mostra come un piccolo aumento del volume cellulare dei globuli rossi che comporta una diminuzione della concentrazione intracellulare di emoglobina avrebbe un effetto terapeutico, considerando l'enorme dipendenza del tempo di ritardo dalla concentrazione di emoglobina.

Chapter I

Introduction

Ia. Sickle cell basics The mutation of a glutamate in the beta chains of the tetrameric hemoglobin molecule (Figure I.1) results in polymerization upon deoxygenation in the tissues to form a viscous gel containing 14-stranded fibers (Figure I.2). The fibers distort the red cells in to a variety of shapes, some with the shape of a sickle from which the disease got its name (Figure I.3). When the cells are reoxygenated in the lungs, the fibers dissolve and the cells return to the normal biconcave disc shape (Figure I.3). Because the cells containing fibers are less flexible, they can become stuck and cause an occlusion that reduces oxygen delivery to the surrounding tissues (Fig. I.4). It is this vaso-occlusion that causes the chronic organ damage of the disease and sporadic episodes so painful that they are called sickle cell crises.

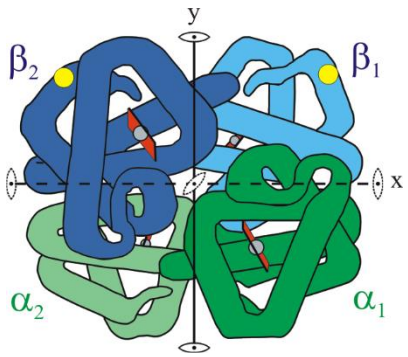

Figure I.1. Schematic of hemoglobin molecule showing location (yellow dots) of glu to val mutation on the molecular surface of the beta subunits (adapted from ref. (1)).

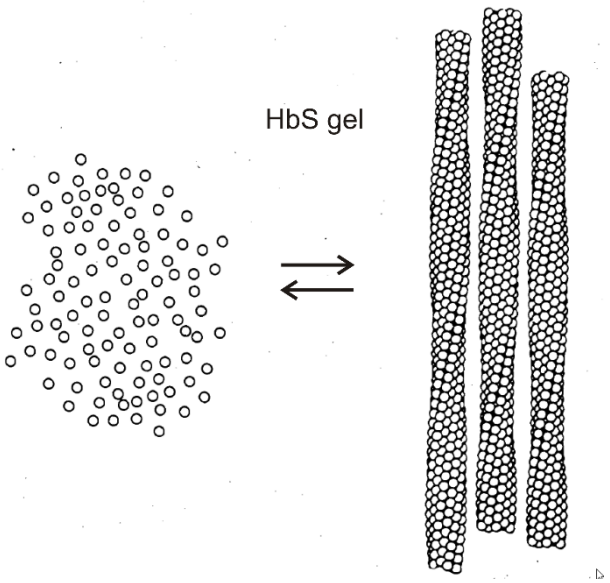

Figure I.2. Hemoglobin S gel. A gel of hemoglobin S consists of a viscous solution of hemoglobin molecules and 14-stranded fibers with no intermediate oligomers. Each circle represents a hemoglobin molecule consisting of 4 subunits.

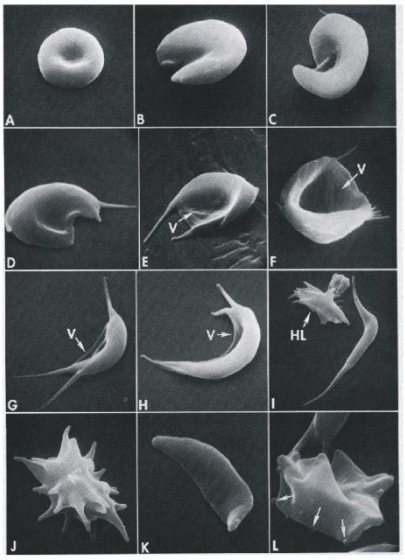

Figure I.3. Scanning electron micrographs of sickle cells. All cells are deoxygenated except in panel A (reproduced from ref (2)).

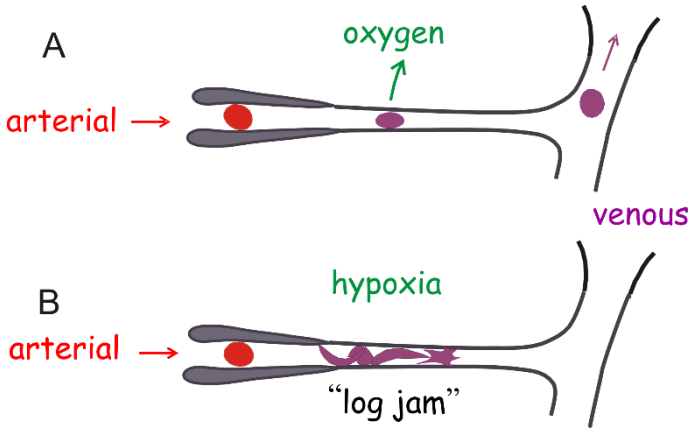

Figure I.4. Schematic of microcirculation - arteriole, capillary and venule . (A) Normal cells squeeze through the narrowest vessels of the tissues, (B) When sickle cells are deoxygenated the fibers that form inside make the cells much less flexible, introducing the possibility that they can become stuck and prevent further passage of cells (the "log jam"), thereby reducing oxygen delivery to the tissues (hypoxia). See Fig. for a more detailed picture.

Ib. Historical Background. Sickle cell hemoglobin is not only the first human disease known to result from a mutant protein (the first "molecular disease") from the landmark work of Linus Pauling (3, 4). It is also the first disease known to be caused by protein aggregation and, consequently, has become a paradigmatic system for the vast amount of current research on protein aggregation associated with neurodegenerative diseases such as Alzheimer's and Parkinson's disease (5-9). Pauling became interested in sickle cell disease when the Harvard hematologist, William B. Castle, told him

about the experiments of a Johns Hopkins medical student, Irving J. Sherman (10). Sherman showed that the oxygenated red cells from patients with this disease have a normal biconcave disc shape, but upon deoxygenation form sickle shapes and exhibit birefringence (Fig. 5), Upon reoxygenation the cells return to a normal biconcave disc shape with the disappearance of birefringence (11).

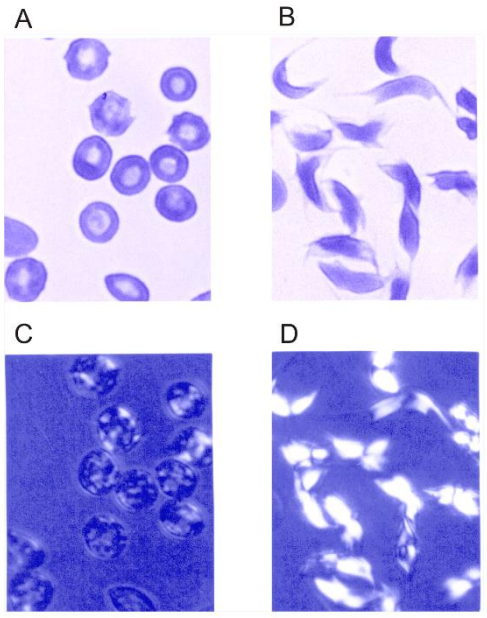

Figure I.5. Optical micrographs of rapidly (seconds) (panels A and C) and slowly (hours) (panels B and D) deoxygenated sickle red cells (reproduced from Eaton and Hofrichter (12)). The micrographs of the cells in panels A and B were obtained with 430 nm linearly-polarized light oriented horizontally, showing greater absorption for cells with the polarization vector perpendicular to their long axis. The micrographs in panels C and D were taken in 450 nm light with the cells between crossed linear polarizers.

Pauling was quite interested in the properties of hemoglobin (13-15) and realized from Sherman's observation of birefringence that the hemoglobin in the red cells from patients with this disease must be aggregated into an ordered structure. In his famous paper showing the difference in electrophoretic pattern of normal and sickle hemoglobin, he also reasoned that the amino acid replacement is on the molecular surface to explain why deoxyhemoglobin S aggregates and that hemoglobin S must have a different conformation when oxygenated to account for the disappearance of birefringence and the return of the normal biconcave disc shape (3). It is, of course, well known that Pauling's brilliant predictions turned out to be correct (16-18). We now know that the birefringence of the aggregated hemoglobin is due to alignment of a 14-stranded solid fiber (19-23) (Fig. I.2).

Chapter II

Thermodynamics of Sickle Fiber Formation

IIa. Control of sickle fiber formation by oxygen: The simplest thermodynamic description of a gel in the absence of oxygen is that it contains only two components, hemoglobin and solvent, and that the polymer phase behaves like a crystal in equilibrium with a solution of hemoglobin molecules, as shown schematically in Fig. I.2. In this description the collection of domains of aligned polymers is viewed as the "crystal," and as such is treated as a separate phase with a constant composition. In the context of this discussion hemoglobin molecules of 64.5 kDa are regarded as monomers. The concentration of hemoglobin monomers in the liquid phase is the solubility, determined by measuring the hemoglobin concentration in the supernatant after sedimenting the fibers in an ultracentrifuge. The solubility is a very accurate measure of the polymer stability. Because the solubility is very high, greater than 160 mg/ml, the solution phase is highly nonideal. This nonideality can be completely accounted for, however, by considering only the hard-sphere excluded volume contributions to the activity coefficient of the monomer. The thermodynamically effective concentration, then is the activity, which is the measured concentration multiplied by the activity coefficient, γ. Activity coefficients are independent of temperature and given by:

$$\gamma = \exp\left(8Vc + 15V^2c^2 + 24.5V^3c^3 + 35.3V^4c^4 + 47.4V^5c^5 + 65.9V^6c^6\right) \qquad (1)$$

where c is the total hemoglobin concentration (either the initial concentration or measured solubility) in g/ml and $V = 0.79$ ml/g is the volume of the equivalent hard sphere (12, 24).

The thermodynamic stability of the fiber as a function of the fraction of the 4 Hb subunits with oxygenated hemes ("fractional saturation" between 0 and 1)) was accurately determined many years ago from careful solubility measurements (25). In these experiments the temperature of a HbS solution at partial saturation with oxygen was increased from 0^oC, where the solution is liquid, to 23.5^oC. After a delay, fibers formed at the elevated temperature resulting in a gel. The gel was then subjected to ultracentrifugation, which sediments the fibers, and allowed optical absorption measurements in the near infrared to determine both the total HbS concentration and fractional saturation of the unpolymerized HbS with oxygen in the liquid supernatant.

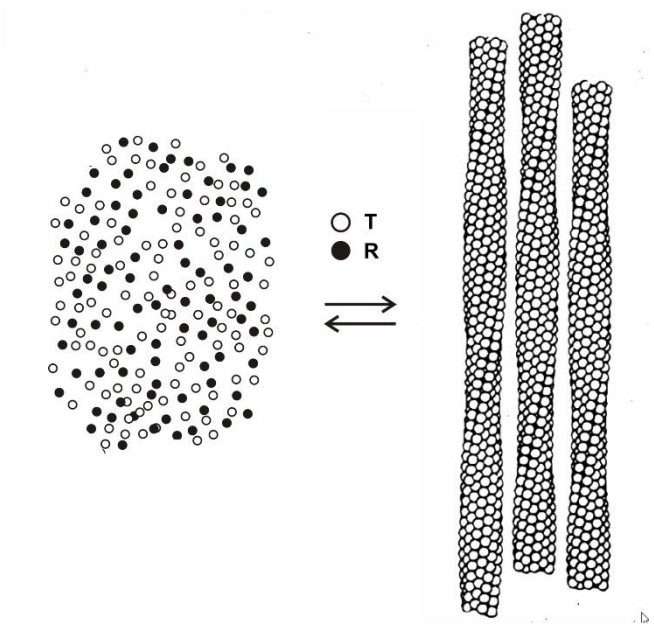

Figure II.1. Schematic structure of gel with HbS partially saturated with oxygen showing that only the T quaternary structure enters the fiber. The total concentration of free HbS tetramers (left) is the solubility and measures the thermodynamic stability of the fiber (right).

Figure II.2 shows the data of Sunshine *et al.* (25) on solubility as a function of the fractional saturation of the liquid phase HbS with oxygen, which remains the most accurate equilibrium data to date. Also shown are the predicted solubilities based on the

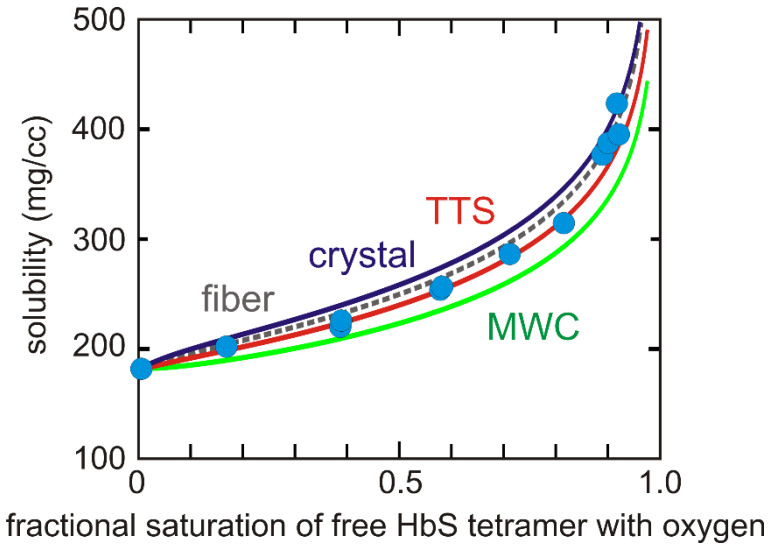

Figure II.2. Solubility of HbS (cyan filled circles) as a function of the fractional saturation with oxygen of the tetramers in the liquid phase and theoretically predicted values based on oxygen binding curves. The filled circles are the measured solubilities. Dashed gray (fiber) curve: solubility calculated from the free tetramer cooperative binding curve (equation 3) and the measured non-cooperative fiber binding curve (25) (K_P = 0.0059 torr^{-1}) using equation 2. The free tetramer cooperative binding curve is taken from the measurements of Gill *et al.* (26) at 25^{o}C using the MWC saturation function (27) (equation 3) with L = 60,500, K_R = 1.47 torr^{-1}, and K_T = 0.016 torr^{-1}. Dark blue (crystal) curve: solubility calculated from the free tetramer cooperative binding curve (equation 3) and the binding curve of the HbA single crystal in T quaternary structure (equation (4) at 25^{o}C (28) (K_P = $K_{crystal}$ = 0.0036 torr^{-1}) using equation 1 . Green (MWC) curve: solubility calculated from the free tetramer cooperative binding curve (equation 2) and the non-cooperative binding curve of free tetramer in the T

quaternary structure with affinity K_T = 0.016 torr^{-1} (equation 5). Red (TTS) curve: solubility calculated from the free tetramer cooperative binding curve (equation 3) and the best least squares fit to the data points using equation (6) of the TTS model (with the known 25°C parameters of K_t = 0.0036 torr^{-1} (28), K_r = 3.7 torr^{-1} (29)) with one adjustable parameter, l_t = 590.. In this fit, the points at saturations greater than 0.85 are the most uncertain and were downweighted by a factor 10 relative to the points at lower saturation.

polyphasic thermodynamic linkage relation of Gill and Wyman between solubility and oxygen binding that satisfies the Gibbs-Duhem relation for a three-component system of hemoglobin, oxygen, and solvent (30). The solubility at each oxygen pressure (p) is related to the fractional saturation of the HbS in the liquid and the polymer phases by (12, 31):

$$\gamma_s c_s \;=\; \gamma_s^0 c_s^0 \exp\left(4\int_0^p \frac{y_s - y_P}{\left(1 - \left[\left(1/c_p - v\right)/\left(1/c_s - v\right)\right]\right)x}\,dx \right) \qquad (2)$$

where y_s and y_P are the fractional saturation as a function of oxygen partial pressure (p) of the free tetramers and fibers, respectively, $a_s = \gamma_s c_s$ is the activity of the free tetramers at pressure p, γ_s is the activity coefficient at concentration c_s, $a_s^0 = \gamma_s^0 c_s^0$ is the activity of the free tetramers at zero oxygen pressure, γ_s^0 is the activity coefficient at concentration c_s^0, c_p is the concentration of hemoglobin in polymer phase (= 0.69 g/cc), and v is the partial specific volume of hemoglobin (= 0.75 cc/g). The term $(1/c_p - v)/(1/c_s - v)$ corresponds to the number of moles of water per mole of hemoglobin in the polymer phase divided by the number of moles of water per mole of hemoglobin in the liquid phase.

The free tetramers of HbS and normal hemoglobin (HbA) have identical cooperative oxygen binding curves, which can be very accurately represented by the Monod, Wyman, Changeux saturation function using the Adair parameters of Gill to generate the binding curve (26).

$$y_s \;=\; \frac{LK_T p\left(1+K_T p\right)^3 + K_R p\left(1+K_R p\right)^3}{L\left(1+K_T p\right)^4 + \left(1+K_R p\right)^4} \qquad (3)$$

The fiber binds oxygen non-cooperatively (25), so its saturation function is simply

$$y_P \;=\; \frac{K_P p}{1 + K_P p} \qquad (4)$$

The fiber binding curve was obtained by measuring the linear dichroism of a gel with known saturation with oxygen of the tetramers in the liquid supernatant to determine the oxygen pressure from equation 3 (25). The linear dichroism is due only to the fibers, as the tetramers free in solution are isotropically oriented and therefore cannot exhibit optical anistropy. Unfortunately, the experimental uncertainties in the measured solubilties were not determined. However, the agreement of duplicate measurements of the most accurate solubilities (i.e. below y_s = 0.85) indicates that the uncertainties are comparable to the width of the circles. Since equation 1 is exact and the activity coefficients are known, the good agreement of the solubilities with the values calculated from the free tetramer and measured fiber binding curve (dashed gray curve) also suggest that the errors cannot be much larger than the plotted width of the circles for the data points at $y_s < 0.85$.

IIb. Theoretical calculation of solubility from MWC and TTS allosteric models. To understand the origin of the low affinity of the fiber used in the calculation of the solubility from equation 2, it is instructive to consider the predictions of the two principle allosteric models - the MWC

model and the tertiary two-state (TTS) allosteric model, which is an extension of the MWC model to include tertiary equilibria within each quaternary structure. The simplest assumption in applying these models is to postulate that only hemoglobin in the T quaternary structure can enter the fiber, as suggested by structural modeling, which show that it is highly unlikely that the oxy (R) quaternary structure can enter the fiber because of multiple steric clashes (32). With this assumption the saturation function for the fiber according to the MWC model is simply:

$$y_P(\text{MWC}) = \frac{K_T p}{1 + K_T p} \qquad (5)$$

where the K_T = 0.016 torr^{-1} is the value for the free hemoglobin tetramers (25, 26). Figure II.2 shows that the MWC model (green curve) does a remarkably good job of reproducing the solubility data without any adjustable parameters other than the value of K_T used to fit the solution binding data, but yields systematically lower values.

The solubility data can be more quantitatively reproduced using the TTS allosteric model, again assuming that only the T quaternary structure polymerizes. In this case, the saturation function is:

$$y_P(\text{TTS}) = \frac{\left(\frac{l_T K_t + K_r}{1 + l_T}\right) p}{1 + \left(\frac{l_T K_t + K_r}{1 + l_T}\right) p} \quad , \qquad (6)$$

where K_t and K_r are the binding constants for the *t* and *r* tertiary structures and l_T is the *t*/*r* population ratio in the T quaternary structure at full deoxygenation. The TTS model postulates that subunits within each quaternary structure have two conformations, a low affinity *t* conformation and a high affinity *r* conformation, and that the affinity of the *t* conformation is the same in T and R, and, similarly, that the affinity of the *r* conformation is the same in T and R (33). Oxygenation and R biases the equilibrium population toward *r*, while deoxygenation and T biases the population toward *t*. Consequently, the *t*/*r* population ratio (l_T) in T is much greater than this population ratio (l_R) in R. The TTS extension of the MWC model was required to explain the discovery of R-like CO binding rates in T (34) and T-like binding rates in R (35). In contrast to the MWC model, which has only a single parameter (K_T) for oxygen binding to the T quaternary structure, the TTS model has three - K_t, K_r and l_T. The values of K_t and K_r are known from binding measurements on the T quaternary structure in a crystal (28) (K_t = 0.0036 torr^{-1}) and encapsulated as R in a silica gel (K_r = 3.7 torr^{-1}) (29). So fitting the solubility curve with the TTS saturation function requires a single adjustable parameter, l_T. The red curve in Figure 2 was calculated from equation 1 using the MWC saturation function (equation 3) for y_s and equation 6 for y_P. The value of l_T that yields the best fit is 590. This value is higher than l_T ~ 200 for the T quaternary structure in solution in the absence of allosteric effectors (29), presumably due to inter-tetramer interactions in the fiber, as in the crystal. These interactions are weaker than those of the deoxyHb A crystal, where the subunits remain in the *t* tertiary conformation upon oxygen binding because l_t is so large, (~ 10^5 (29)) and equation (6) reduces to equation (4) with a binding constant of K_t.

IIc. Theoretical calculations of solubility in mixtures of HbS with normal and fetal hemoglobins. For the mixtures of HbS with normal (HbA) or fetal (HbF) hemoglobins, the solubilities as a function of fractional saturation with oxygen can be calculated from: (Derived in Appendix A):

$$\left[ZB_1 + B_2 - (1-X_A)^2 ZB_3 \right]\left[Ze_2B_1 + B_2 \right] - \left[2X_A(1-X_A) \right]\left[ZB_1 + B_2 \right] Ze_2B_3 = 0$$

$$B_1 \equiv c_P(c_0 - c_s),\ B_2 \equiv \Gamma c_s^0 (c_P - c_0),\ B_3 \equiv c_0(c_P - c_s) \qquad (7)$$

with

$$Z = \frac{L(1+K_P p)^4}{L(1+K_T p)^4 + (1+K_R p)^4} \qquad (8)$$

The solubility, c_s, for a given fraction of HbA or HbF (X_A or X_F), total initial Hb concentration, c_0, and liquid phase fractional saturation, y_s calculated for each pressure, p, from equation (3) is found by finding the value of c_s that yields zero for the sum of the two terms on the left-hand side of equation (7). For HbS/HbA mixtures $e_{\alpha_2\beta_2^A} \equiv e_3 = 0$ and $e_2 = 0.4$ for copolymerization of the hybrid tetramer $\alpha_2\beta^S\beta^A$ (12). For HbS/HbF mixtures, the co-polymerization probability for both the $\alpha_2\gamma_2$ HbF homotetramer, $e_{\alpha_2\gamma_2} \equiv e_3$, and hybrid tetramer, $\alpha_2\beta^S\gamma \equiv e_2$ are zero, since only the $\alpha_2\beta_2^S$ tetramer enters the fiber, and equation (7) reduces to:

$$X_F^2 c_0 Z(c_P - c_s) - 2X_F c_0 Z(c_P - c_s) + (c_P - c_0)\left(Zc_s - \Gamma c_s^0\right) \qquad (9)$$

IId. Relevance of solubility to pathophysiology of sickle cell disease. As shown in Figure II,3**,** it is useful to think of the measured solubilities as a boundary line that separates the two phases of a HbS solution *at equilibrium*. Solutions containing HbS concentrations that lie above the line will contain fibers. If a sufficient fraction of the HbS is polymerized, the increase in viscosity will make the red cells significantly less flexible. Solutions of concentrations below the line will remain liquid with no fibers *at equilibrium*. These red cells will never sickle and have normal flexibility.

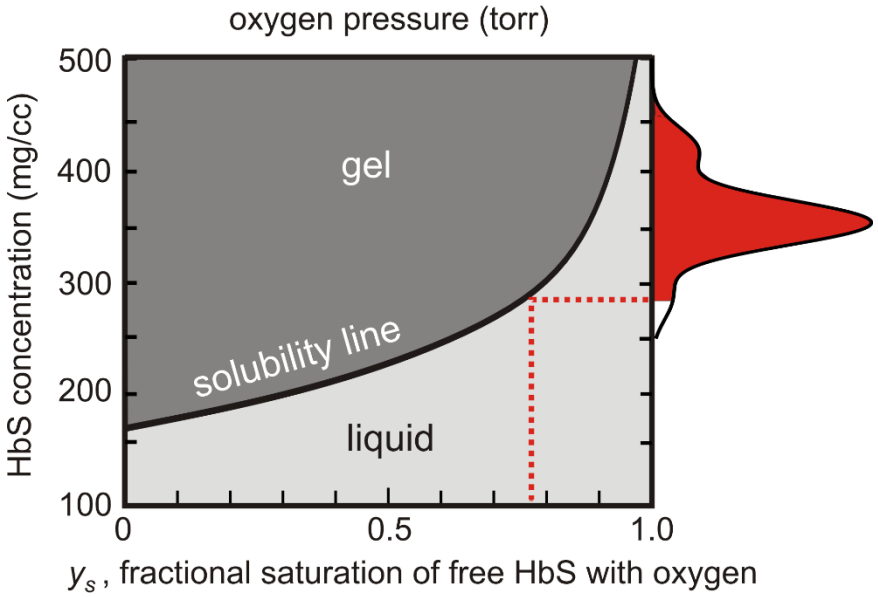

Figure II.3. Physiological concentration-saturation phase diagram at 37°C. The solution contains fibers *at equilibrium* for all values of the HbS concentration and fractional saturation of the Hb tetramers in the liquid phase above the solubility line. *In vivo*, the distribution of intracellular HbS concentrations vary from 250 mg/ml to more than 450 mg/ml, while the saturation of HbS decreases to 40 torr or less in most tissues (36), corresponding to a hemoglobin saturation with oxygen in the liquid phase of about 75%. The red shaded area of the concentration distribution shows that almost every cell would contain fibers in the tissues *at equilibrium*. The concentration distribution on the right-hand *y*-axis is the same as in Fig. II.4 and is a representative of distributions for homozygous SS patients.

The distribution of intracellular hemoglobin concentrations in sickle blood is quite variable and ranges from 250 mg/ml to more than 450 mg/ml (37) (Figure II.4). The concentration distribution is broader than found for normal red cells because of two

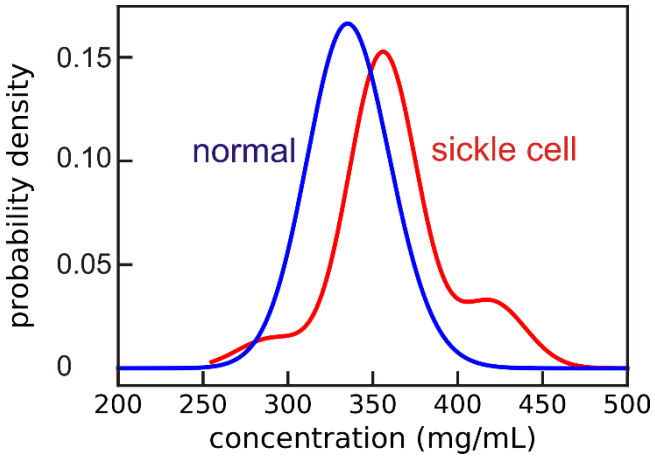

Figure II.4. Intracellular total hemoglobin concentration distribution for red cells from normal patients (average of 22 patients from ref. (38)) and a concentration distribution representative of distributions for homozygous SS patients.

effects. The destruction of damaged red cells stimulates erythropoiesis that results in release of immature red cells (reticulocytes) having a low intracellular hemoglobin concentration (39), while repeated cycles of sickling and unsickling cause the loss of potassium ions and water that result in red cells with a higher concentration than found in normal blood (40). There is, unfortunately, very little data on the oxygen pressures or fractional saturation of hemoglobin in oxygen in tissues of humans. However, experiments on animals suggest that the oxygen pressure decreases to less than 40 torr in the tissues (36), corresponding to less than 75% saturation with oxygen (p50 = 27.5 torr, Hill n =2.9). Thus, at the oxygen saturations of HbS in the tissues *in vivo*, the phase diagram (Figure 4) shows that almost every cell would contain fibers if HbS polymerization were at equilibrium.

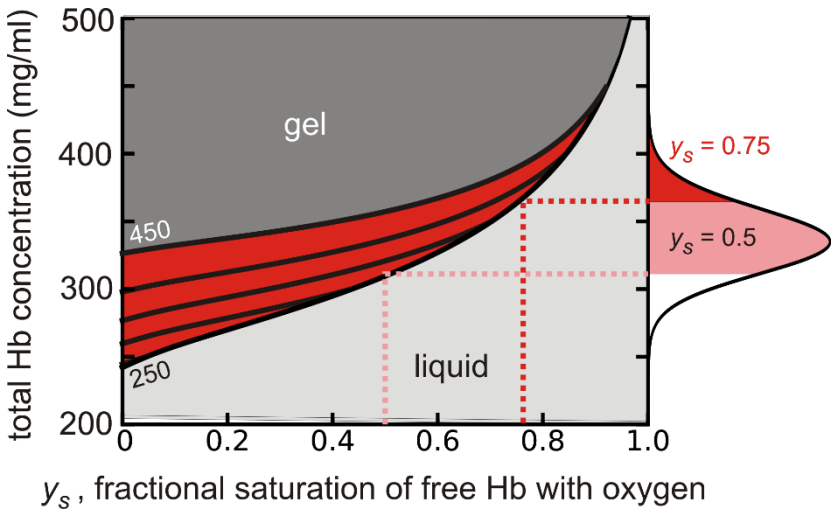

Figure II.5. Physiological concentration-saturation phase diagram at 37°C for a 62/38 HbA/HbS mixture. Solubilities were calculated from equation 7. The solubility (black curves at intervals of 50 mg/ml, from 250 mg/ml to 450 mg/ml every) increases with increasing total Hb concentration because the species $\alpha_2\beta^A{}_2$ and $\alpha_2\beta^S\beta^A$ build up in the liquid phase as the total Hb concentration increases due to lack of copolymerization $\alpha_2\beta^A{}_2$ and only partial copolymerization $\alpha_2\beta^S\beta^A$. The solution contains fibers *at equilibrium* for all values of the total Hb concentration and fractional saturation of the free Hb tetramers in the liquid phase above the lowest black curve. *In vivo*, the distribution of intracellular HbS concentrations vary from 250 mg/ml to ~400 mg/ml (Figure 5), while the saturation of HbS decreases to 40 torr or less in most tissues (36), corresponding to a hemoglobin saturation with oxygen in the liquid phase of about 75%. The red shaded area in the concentration distribution on the right y-axis shows the fraction of trait cells containing fibers *at equilibrium* when the liquid phase is 75% saturated with oxygen, while the pink plus red shaded areas show the fraction of trait cells containing fibers when the liquid phase is 50% saturated with oxygen. The concentration distribution is the average of 22 normal patients (38).

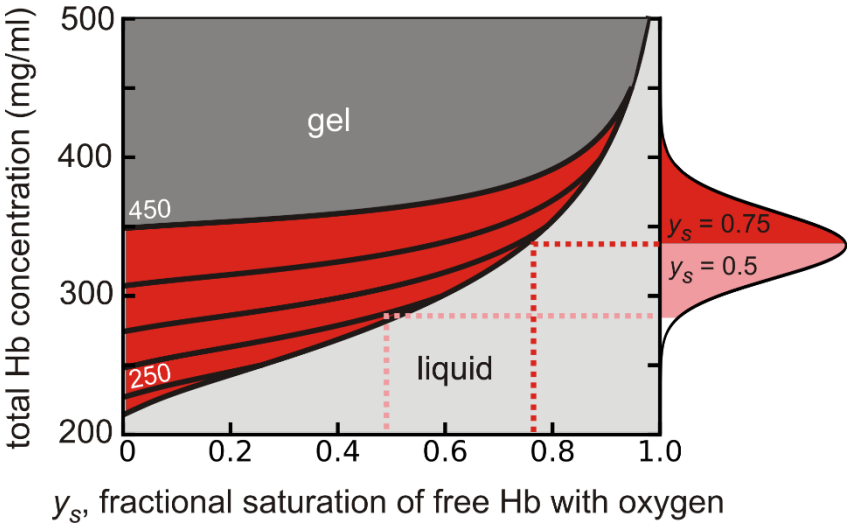

Figure II.6. Physiological concentration-saturation phase diagram at 37°C for a 30/70 HbF/HbS mixture as is found in S/HPFH. Solubilities were calculated from equation 9. The solubility (black curves at intervals of 50 mg/ml, from 250 mg/ml to 450 mg/ml every) increases with increasing total Hb concentration because the species $\alpha_2\gamma_2$ and $\alpha_2\beta^S\gamma$ do bot copolymerize and build up in the liquid phase as the total Hb concentration. The solution contains fibers *at equilibrium* for all values of the total Hb concentration and fractional saturation of the free Hb tetramers in the liquid phase above the lowest black curve. *In vivo*, the distribution of intracellular HbS

concentrations vary from 250 mg/ml to 450 mg/ml (Figure 5), while the saturation of HbS decreases to 40 torr or less in most tissues (36), corresponding to a hemoglobin saturation with oxygen in the liquid phase of about 75%. The red shaded area in the concentration distribution on the right y-axis shows the fraction of S/HPFH cells containing fibers *at equilibrium* when the liquid phase is 75% saturated with oxygen, while the pink plus red shaded areas show the fraction of S/HPFH cells containing fibers when the liquid phase is 50% saturated with oxygen. The concentration distribution is the average of 22 normal patients (38).

The phase diagram for sickle trait in Figure II.5 shows that at 75% saturation of the free tetramers, a significant fraction of cells would contain fibers, while at 50% saturation a majority of cells would contain fibers. In the case of S/HPFH (Figure II.6, approximately half would contain fibers at 75% saturation and at 50% saturation, almost every cell would contains fibers.

Chapter III

Kinetics of Cell Sickling

IIIa. Calculation of sickling kinetics *in vivo* at tissue oxygen pressures for patients with homozygous sickle cell (SS) disease. Because of the unusual kinetics, with a delay period prior to fiber formation, polymerization is very far out of equilibrium. Consequently, the phase diagrams describing the equilibrium properties do not apply to the situation *in vivo*. Unfortunately, there are currently no experiments on delay times for individual cells that are deoxygenated on a physiological time scale to partial oxygen saturations of the hemoglobin. Moreover, there is very little detailed information on tissue saturations in humans and none on deoxygenation rates. However, given a rate of deoxygenation to a final saturation and an intracellular HbS concentration distribution, we can provide a partial answer to this question by theoretically calculating the fraction of cells that will sickle as a function of time.

Because the oxygen pressure is changing with time, the delay time (t_d) is also changing. The time at which fibers form inside a cell, i.e. the sickling time (t_{sickle}), occurs when

$$\int_0^{t_{sickle}} \frac{d\tau}{t_d(\tau)} = 1, \qquad (8)$$

This relation of A. Szabo, derived in the Appendix B, shows that the sickling time (t_{sickle}) is determined if the delay time (t_d) as a function of time (τ) is known (notice that for a time-independent delay time, i.e. t_d constant, $t_{sickle} = t_d$). The key to this calculation, described in detail in the Appendix B, is the recent discovery of a universal relation between the delay time and the supersaturation of the solution (the ratio of the total concentration of Hb to the equilibrium solubility, each multiplied by an activity coefficient (equation 2)) (41). The delay time for each cell depends on the supersaturation (Appendix C), which depends on the intracellular HbS concentration (Figure II.4) and the solubility, which depends on the fractional saturation of HbS with oxygen (Figure II.2) that is changing with time as the saturation decreases. Knowing the solubility as a function of oxygen saturation (Figure II.2) and the universal relation between the delay time prior to fiber formation and the activity supersaturation, we can calculate the fraction sickled with time for every cell for various rates of deoxygenation of the hemoglobin to various final oxygen saturations.

There is one experimental data set that can be used to make a qualitative comparison with our calculation of the fraction sickled as a function of time. Mozzarelli *et al.* (42) used a cw laser to create intracellular hemoglobin at known partial saturations with carbon monoxide from optical absorption measurements with a microspectrophotometer, by using a CW laser to partially photodissociate carbon monoxide (CO) in CO-saturated SS cells. The experiments are perfectly relevant to sickling at partial saturation with oxygen, because the allosteric equilibrium properties of HbS+CO and HbS+O_2 are identical except for the absolute affinities. The experimental data consists of both the fraction sickled as a function of saturation of the intracellular HbS with CO at 600 sec after laser photodissociation with a desaturation half-time of ~300 sec and the fraction sickled as a function of saturation after allowing CO to recombine to a cell that has been 100% desaturated. The latter represents the fraction containing fibers ("sickle") *at equilibrium*, since there is no delay in the melting of fibers upon binding CO, which occurs in seconds. The determination of whether or not a cell contains fiber at a given saturation is determined by rapidly increasing the laser intensity to completely photodissociate the CO. If there is a delay time, the cell contains no fibers. Cells that exhibit no delay time contain fibers.

Given the enormous sensitivity of the kinetics to concentration distributions, described in detail below, and recognizing that the distribution in the experiment of Mozzarella et al. could be quite different than our representative SS distribution (Fig. II.4), the fact that the measured and calculated fractions sickled are even roughly similar must taken as strong support for the validity of the calculations.

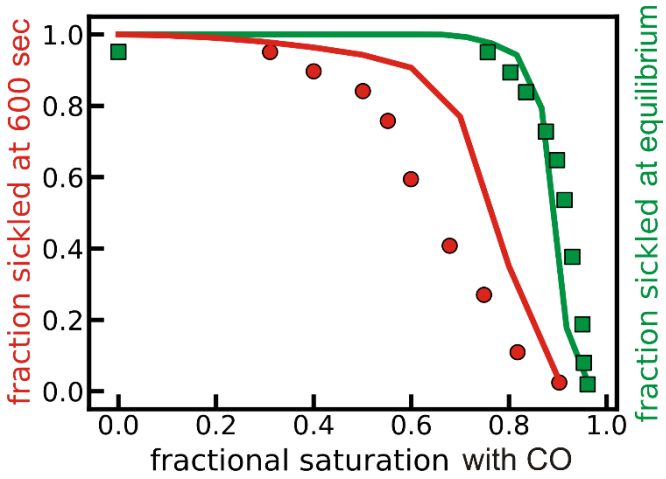

Figure III.1. Comparison of measured (42) and calculated fraction containing fiber ("sickled") at 600 sec after a 300 sec desaturation of the HbS carbon monoxide complex. Red circles and green squares are Mozzarelli experimental results, while the red and green curves are calculated.

There is no information on oxygen pressures or deoxygenation times in the microcirculation of humans. However, measurement of oxygen saturation in the venous returns from human organs and measurements of oxygen partial pressures and deoxygenation rates in animals suggest that the most relevant *in vivo* values for our calculations of sickling in the circulation of SS patients are saturations of more than 50% and deoxygenation times of ~ 1 sec (43). Assuming that the transit time through the arterioles and capillaries is ~1 sec, our calculations (Fig. III.2) indicate that <20% of the cells would sickle in the microcirculation, while >80% of cells without fiber formation. The results are very sensitive to the concentration distribution, so variations in the concentration distributions alone is predicted to result in a wide patient-to-patient variation in the *in vivo* kinetics and could be at least part of the origin of variation in clinical severity.

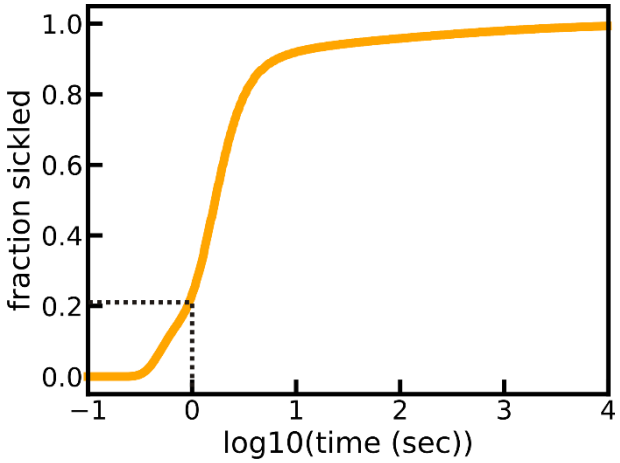

Figure III.2. Calculation described in Appendix D for a 1 sec desaturation time to 50% saturation with oxygen of the liquid phase for the representative SS distribution of Fig. II.4. The fraction sickled at 1 sec is ~20%.

IIIb. Calculation of sickling kinetics *in vivo* at tissue oxygen pressures for patients with sickle trait and S/HPFH. Figure III.3 shows the results of calculations of fraction sickled vs time for trait and S/HPFH. The only difference in the calculation from those for SS blood is that the solubility at each fractional saturation with oxygen depends on the total Hb concentration. At 50% saturation sickling times are longer than both the transit times through the microcirculation and the total circulation time (~30 sec).

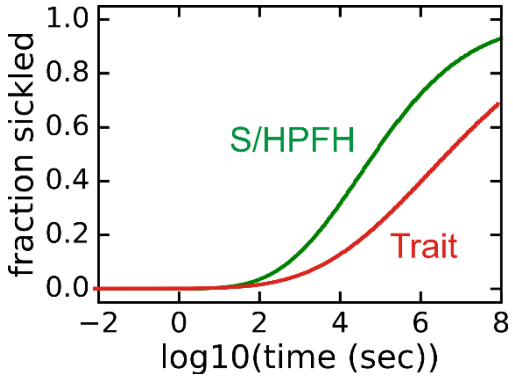

Figure III.3. Calculation described in Appendix D for a 1 sec desaturation time to 50% saturation for sickle trait and for S/HPFH.

IIIc. Conclusions from calculations of *in vivo* sickling kinetics. Although using an equilibrium analysis alone to discuss pathophysiology (44, 45) and therapy (46), has often been done, it is very misleading. However, because of the relation between the delay time and supersaturation (Fig. A1), which depends on the solubility (c_s), the delay time increases and the fraction polymerized decreases as the solubility increases. Consequently, even though the calculated fraction polymerized rarely occurs *in vivo*, its relation to the kinetics allows it to make a meaningful correlation of hemoglobin composition and concentration of red cells in the various sickle syndromes with clinical severity (48, 49). This is made quite clear from examination of the concentration-saturation phase diagrams in Figures II.3, II.5, and II.6. The phase diagram for homozygous SS cells shows that almost every cell would be sickled in the tissues even at saturations with oxygen as high as 75% (Fig. II.3). Consequently, if fiber formation were at equilibrium, it is unlikely that patients would survive after the replacement of fetal hemoglobin with adult HbS, which is complete at about 6 months (47). In the case of sickle trait, the phase diagram shows that while only a small fraction of cells would sickle at 75% saturation, the majority would be sickled at 50% saturation. Moreover, many more would be sickled in the hypertonic renal medulla. In S/HPFH, about half the cells would be sickled at equilibrium at 75% saturation and almost every cell would be sickled at 50% saturation. Consequently, the phase diagrams for sickle trait and S/HPFH suggest that both conditions would be associated with severe pathology were fiber formation at equilibrium, while both conditions are considered benign relative to sickle cell disease (46).

Oxygen binding is close to equilibrium as red cells pass through the tissues because the dissociation and binding rates are much faster than the transit time. As a result, the oxygen binding measurements measured on the tens of minutes time scale that began over 100 years ago (50) have physiological significance even though deoxygenation in the tissues and reoxygenation in the lungs occurs much faster. In sharp contrast, polymerization of HbS *in vivo* in homozygous SS disease is very far out of equilibrium because the kinetics of fiber formation for the majority of cells are slower than the transit times through the narrowest vessels of tissues. In spite of the lack of detailed data on *in vivo* deoygenation rates and tissue oxygen pressures, the conclusion from Figure III.2 is unambiguous. The vast majority of cells entering the microcirculation with fully oxygenated HbS escape before fibers

form. Indeed, it is the delay before fibers form (Figure I.4) that allows most cells to escape the narrow vessels before sickling occurs, which makes the disease survivable. The result in Figure III.2 indicates that only 20% of cells sickle in the microcirculation with tissue oxygen saturation of 50%. This is similar to the results of calculations by Ferrone and coworkers (43). However, the agreement is somewhat fortuitous because of at least partial cancellation of two effects. Ferrone and coworkers assumed instantaneous desaturation, which decreases the sickling time (equation 8) and employed a concentration distribution with much lower concentration, which results in longer sickling times. The reason for the distribution with lower concentrations calculated by Coletta *et al*. (51), from their delay time distribution for SS cells may in part have been due to inherent bias in the experiment, where measurements were not performed on distorted cells saturated with carbon monoxide. Such cells, called "irreversibly sickle cells", contain the highest intracellular Hb concentrations (52).
Moreover, both sickle trait and S/HPFH are benign conditions because, with the exception of the hypertonic renal medulla, cells rarely sickle *in vivo* (Fig. III.3).

The events in the microcirculation are most probably more complicated than depicted in Figure I.4. Figure III.4 shows the possible scenarios that have been proposed.

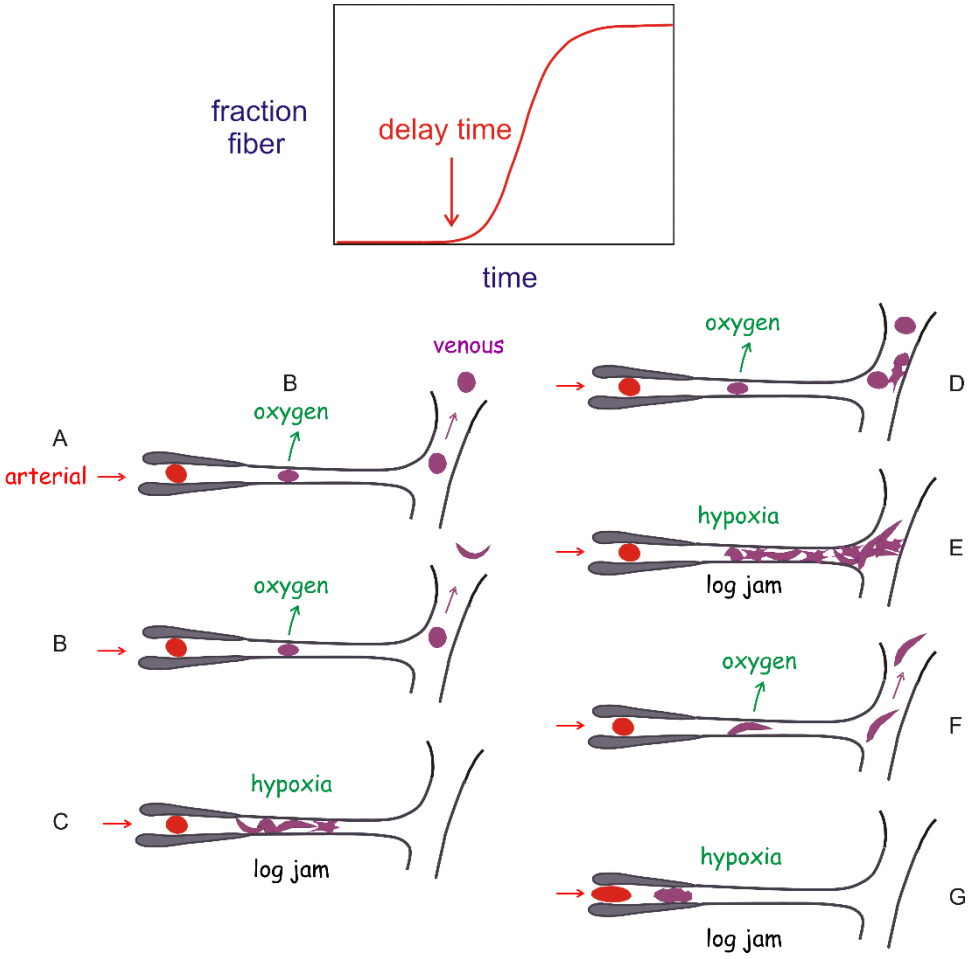

Fig. III.4. Connection between fiber formation kinetics and pathophysiology of sickle cell disease. Upper panel: schematic of kinetic progress curve for fiber formation. The delay time is extraordinarily sensitive to HbS concentration, depending on the 30th power of the concentration, possibly the largest concentration dependence ever observed for a chemical reaction. Thus, for example, an 8% decrease in the Hb concentration will result in a 10-fold increase in the delay time (Recall for a bimolecular reaction, an 8% decrease in reactants will produce an 8% increase in the half-time for the reaction). Lower panels: schematic of microcirculation showing an arteriole, capillary and venule, and various sickling scenarios. The site or sites of occlusion have not been definitively established. However, animal models (53) and rheological studies (54) of sickled cells suggest that

the major site of occlusion is in the venules and not in the narrower capillaries (55). Factors that slow the transit of red cells through the microcirculation, such as increased adherence to the vascular endothelium by red cells that are damaged form sickling/unsickling cycles or increased leukocytes associated with infection, will increase the probability of vaso-occlusion (56-58).Scenario (A) The delay time is so long that the red cell squeezes through the narrow capillary and returns to the lings and become reoxygenated before any fibers form to produce cellular distortion ("sickling") and decreased flexibility. (B) Sickling occurs in larger vessel and returns to the lungs where the fibers melt and the cell unsickles. (C) Fibers form while the cell is in the capillary and becomes stuck, causing a log jam effect and decreased oxygen delivery to the surrounding tissue (hypoxia). (D) Unsickled cell escapes both the capillary and the post-capillary venule where sickled cells are adherent to the venule endothelium. (E) Cell sickles and cannot escape the post-capillary venule, where sickled cells are adherent, causing a log jam. (F) Cell sickles in capillary, but nevertheless squeezes through to the larger vessels. (G) Cell sickles before or within the pre-capillary arteriole because the concentration of intracellular hemoglobin is very high or nuclei are already present because fibers have not completely melted upon oxygenation in the lungs, enormously decreasing the delay time (42).

The question for future studies is apparent from Figure III.4. What is the relative fraction of each of these scenarios in sickle cell patients, and how do the fractions change in sickle cell crisis? Since the transit time is a critical factor in any kinetic analysis, it raises the question of the origin of the wide range of clinical severity in sickle cell disease. Does it result primarily from patient-to-patient variations in sickling times or transit times? Clinical studies comparing clinical severity with distributions of red cell sickling times and adherence, which slows transit times, could potentially answer this important question.

Chapter IV

Five Approaches to Treating the Disease by Inhibiting Fiber Formation with a Drug (59)

IVa. Introduction. Most of the non-genetic approaches currently in clinical trials are aimed at using drugs to ameliorate the downstream sequelae of sickle hemoglobin (HbS) polymerization, such as adhesion of red cells to vascular endothelium, leukocytes and platelets, as well as inflammation, coagulation and nitric oxide scavenging (56, 60-63). Indeed, there is strong rationale for thorough investigation of these phenomena, and therapeutic applications are beginning to bear fruit. For example, the administration of GMI-1070, a pan-selectin inhibitor, appears to shorten the duration of acute sickle pain crises accompanied by a marked reduction in opioid use (64). Moreover, a recent randomized double-blinded study found that monthly administration of a monoclonal antibody against P-selectin was effective in lowering the frequency of sickle pain crises (65). Although these therapeutic interventions do not appear to be significantly superior to hydroxyurea, they could be effective in combination. Moreover, other attempts to target downstream sequelae have thus far proven to be even less effective (66-73).

More bench research and clinical trials should be directed toward the polymerization process itself, the root cause of sickle cell pathology. The purpose of this chapter is to briefly describe the biochemical and biophysical basis of five distinct approaches to inhibit polymerization for treating sickle cell disease and to discuss their connection to the anti-polymerization drugs currently in clinical trials. Before considering different ways of decreasing fiber formation, it is important to point out that therapeutic benefit does not require complete inhibition of HbS polymerization. Even small degrees of polymerization inhibition can produce large increases in the delay time, allowing many more cells to escape the tissues without sickling (74). Moreover, transient changes in the delay time probably contributes importantly to the episodic nature and unpredictability of sickle cell crises (75). Thus, the probability of sickling in the microcirculation is decreased if either the delay time is increased(74, 76) or the transit time through the microcirculation is decreased, which is the therapeutic rationale for reducing adhesion of blood cells to the vascular endothelium (56, 60, 61, 63).

IVa. Block intermolecular contacts in the sickle fiber. One of the important early milestones in sickle cell research was the construction of a detailed molecular model of the fiber structure (Fig. IV.1). The structure is based on image reconstruction of transmission electron micrographs (Fig. IV.1A) (20), the X-ray structure of deoxy HbS (19) (Fig. IV.1B) and the determination of residues that participate in an intermolecular contact from polymerization studies on mixtures of HbS with other naturally occurring hemoglobins containing mutated residues on the molecular surface (77, 78). The 21 nm diameter fiber is constructed of 14 strands, consisting of 7 helically twisted strand pairs found in the X-ray structure of deoxyHbS (Fig. IV.1C). The polymerization studies of mixtures positioned the X-ray determined double strands in the fiber to define the inter-double strand contacts.

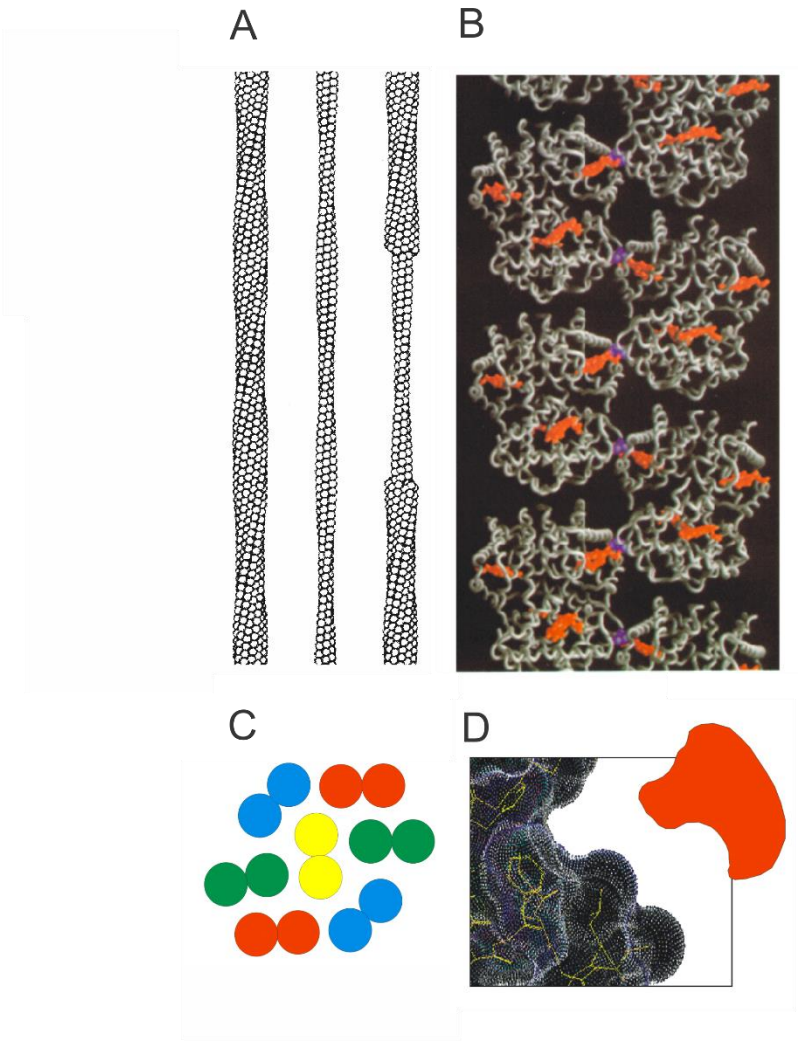

Figure IV.1. Sickle fiber structure from ref. (59). (A) Low resolution structure of 14-stranded solid fiber determined by electron microscopy (20). Each HbS tetramer is a single circle. (B) Atomic structure of deoxy HbS determined by X-ray crystallography (19) showing that one of the two beta 6 valines (purple) in each tetramer makes an inter-molecular contact with adjacent strand close to the pocket containing the hemes (orange). (C) Cross-section of sickle fiber composed of 7 double strands. (D) Cartoon of small molecule inhibitor that could fit into the shallow acceptor site for the beta 6 valine.

A common approach to drug development is to identify a protein target and screen compounds that bind tightly to a specific site on the protein, such as the active or, more recently, allosteric site of an enzyme. The analogous approach for treating sickle cell disease would be to find a small molecule that has a high affinity for a site on the surface of the HbS molecule that is involved in an intermolecular contact in the fiber. The problem in using this approach for sickle cell disease is three-fold. First, the drug must have a high degree of specificity for binding to hemoglobin. Secondly, there is almost one pound of hemoglobin in the average patient with homozygous sickle cell disease, so unless the binding is extremely strong, as in a covalent bond, a very large amount of drug would be required. The third concern is that the surface of the hemoglobin molecule is smooth, with no residues involved in an intermolecular contact available for stereospecific covalent attachment of an inhibitor and no apparent deep clefts or crevices that would be required for tight, non-covalent binding (Fig. IV.1D). However, transient openings in the structure for drug targeting might be discovered using all-atom molecular dynamics simulations, a method currently being used to find binding sites for drug targeting that are not obvious from static X-ray structures (79). Consequently, although much more challenging than the more common empirical drug targeting, this approach should not be discounted.

IVb. Induce fetal hemoglobin synthesis. The symptoms of sickle cell disease do not appear until several months after birth when most of the fetal hemoglobin (HbF) is replaced by HbS. Moreover, as mentioned above, the compound heterozygous condition of sickle cell disease with pancellular persistence of fetal hemoglobin (S/HPFH) is a relatively benign condition. Importantly, in S/HPFH, the HbF is homogeneously distributed. These "F cells" all contain about 30% HbF and 70% HbS (46). In contrast, in SS disease HbF is heterogeneously distributed with 34 ± 17 % F cells and no detectable HbF in the remaining 65% (80). Following hydroxyurea therapy at maximum tolerated doses, the fraction of F cells rises to 48 ± 23 % while the fraction of HbF increases even more. Thus hydroxyurea therapy results in an increase in HbF per F cell. The drug would be more effective if the increase in HbF were distributed among a greater fraction of red cells (81). The focus of current research in this area, therefore, is to induce HbF synthesis in as many red cells as possible(82). One promising approach is the selective inhibition of the transcription factor BC11A which dramatically increases the expression of γ globin (83, 84).

Because of the enormous sensitivity of the kinetics of polymerization to $\alpha_2\beta^S_2$ concentration, the beneficial effect of HbF results primarily from the decrease in the intracellular concentration of the HbS homotetramer, $\alpha_2\beta^S_2$ (85). This inhibitory effect, however, is quite complex (12) (Fig. IV.2). Dissociation of tetramers into $\alpha\beta$ dimers and random

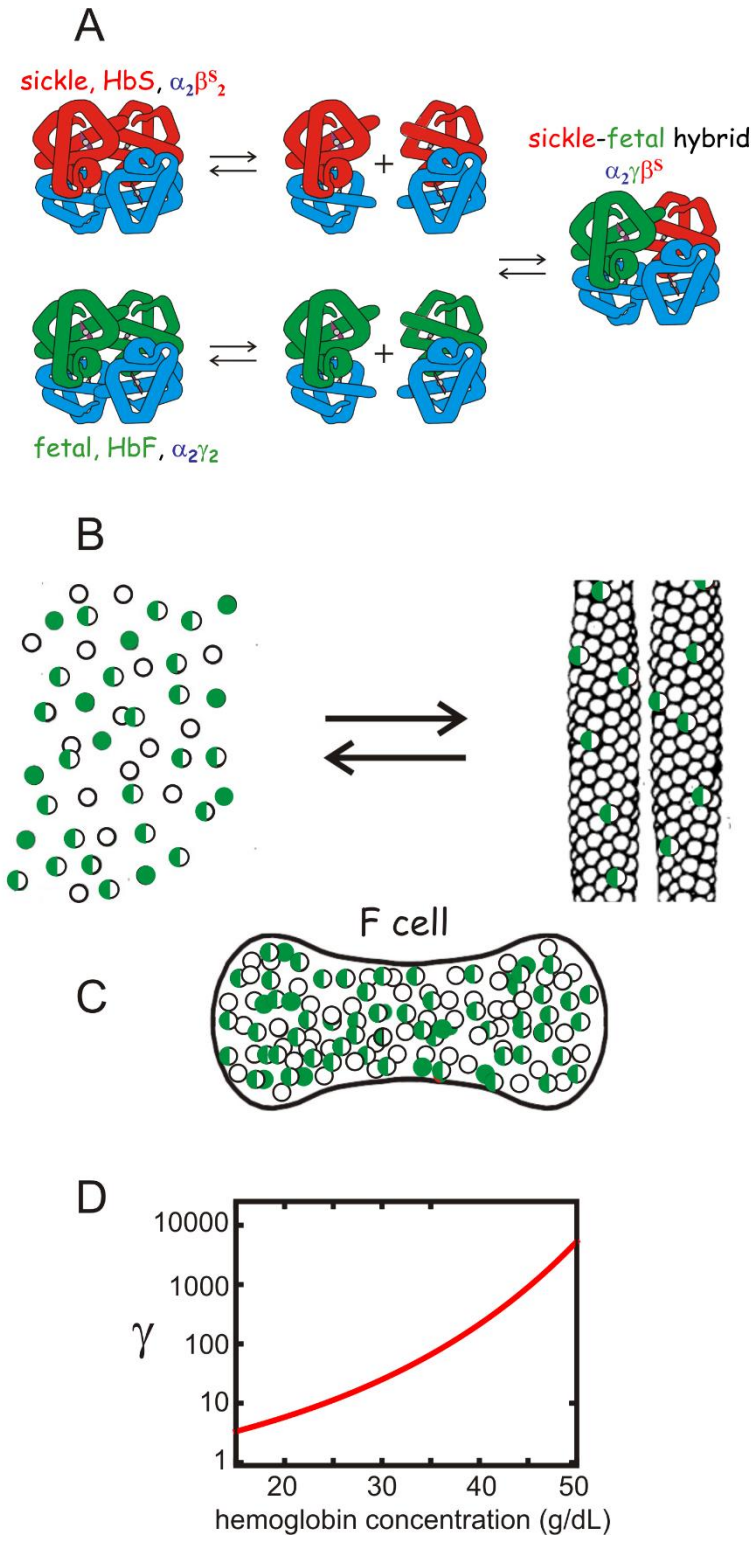

Figure IV.2. Mechanism of inhibition of polymerization by fetal hemoglobin from ref. (59). (A) Dissociation of tetramers into $\alpha\beta$ dimers and reassociation in mixtures of HbS and HbF results in 3 tetramers in a binomial distribution, thereby further lowering the fraction of the HbS homotetramer ($\alpha_2\beta^S{}_2$)(86). (B) Cartoon of polymerization equilibrium in HbS/HbF mixture. As in a crystallization reaction, hemoglobin tetramers are present in two phases - the liquid phase (left) or the fiber phase (right). The fibers that form in these mixtures are primarily composed of the HbS homotetramers, but there is also some copolymerization of hybrid tetramers ($\alpha_2\beta^S\gamma$) (half-green, half-empty circles).(12, 87) (C) Cartoon of F cell with 30% HbF and 70% HbS. The excluded volume effect of the non-copolymerizing $\alpha_2\gamma_2$ tetramer (full green-filled circles) and partially copolymerizing

tetramer $\alpha_2\beta^S\gamma$ (half-green, half-empty circles) increases the activity of the polymerizing $\alpha_2\beta^S{}_2$ homotetramer (empty circles) (D) Activity coefficient (γ) as a function of total Hb concentration. The unitless activity coefficient is the factor that multiplies the measured concentration (i.e. moles per liter or grams per deciliter) to obtain the "activity", which is the thermodynamically-effective concentration.(88)

reassociation results in a binomial distribution of tetramers, reducing the concentration of the $\alpha_2\beta^S{}_2$ homotetramer further.(86) (Fig. IV.2A). A mixture of 70% HbS and 30% HbF, for example, contains 3 tetramers with a binomial distribution, 49% $\alpha_2\beta^S{}_2$, 9% $\alpha_2\gamma_2$, and 42% $\alpha_2\gamma\beta^S$.

Two other effects must be considered in addition to tetramer-dimer dissociation and reassociation. One is copolymerization of the $\alpha_2\gamma\beta^S$ hybrid tetramer (Fig.IV.2B) (87, 89), which can enter the fiber, but to a much lesser extent than the $\alpha_2\beta^S{}_2$ homotetramer or even the $\alpha_2\beta^S\beta^A$ hybrid tetramer because in the γ subunit threonine at position 87 is replaced by a glutamine, which forms a much less favorable critically-important intermolecular lateral contact with valine 6. The second effect on the $\alpha_2\beta^S{}_2$ concentration decrease is the large non-ideality in the concentrated HbS solution within the red cell. The thermodynamically effective concentration of $\alpha_2\beta^S{}_2$, called the activity, is not the measured concentration in moles or grams per unit volume, but rather the concentration multiplied by a correction factor, the activity coefficient (γ) (Fig. IV.2D). The activity coefficient accounts for the fact that the non-copolymerizing tetramers take up space in the solution and decrease the volume accessible to the polymerizing tetramers. This so-called "excluded volume" effect is extremely large and must be considered in all thermodynamic and kinetic descriptions of polymerization.(41, 88, 90-92) The activity at the concentration of 35 g/dl, a typical MCHC, for example, is almost 100-times greater than the measured concentration. The net result of this effect is that the activity of $\alpha_2\beta^S{}_2$ in the solution phase at equilibrium is increased, making the decrease in the concentration of the $\alpha_2\beta^S{}_2$ tetramer less effective in increasing the delay time than by simply increasing red cell volume by means of osmotic or ionophoric dilution discussed below.

IVc. Increase oxygen affinity. The results of studies on the control polymerization by oxygen can be explained by applying the famous two-state allosteric model of Monod Wyman and Changeux (MWC) (Fig. IV.3) and discussed in detail in Chapter II (27, 93). According to the model of MWC, there is an equilibrium between a low oxygen affinity arrangement of the 4 subunits of fully deoxyhemoglobin - the T quaternary structure - and a high affinity arrangement of fully oxygenated Hb - the R quaternary structure (Fig. IV.3A). As discussed in Chapter II, solubility measurements of concentrated solutions of HbS as a function of the saturation of hemoglobin with oxygen in the solution phase can be almost quantitatively explained by not allowing the R quaternary structure to enter the fiber. Moreover, the sickle fiber binds oxygen with an affinity that is only slightly higher than the affinity of the T quaternary structure in the crystal (25, 29).

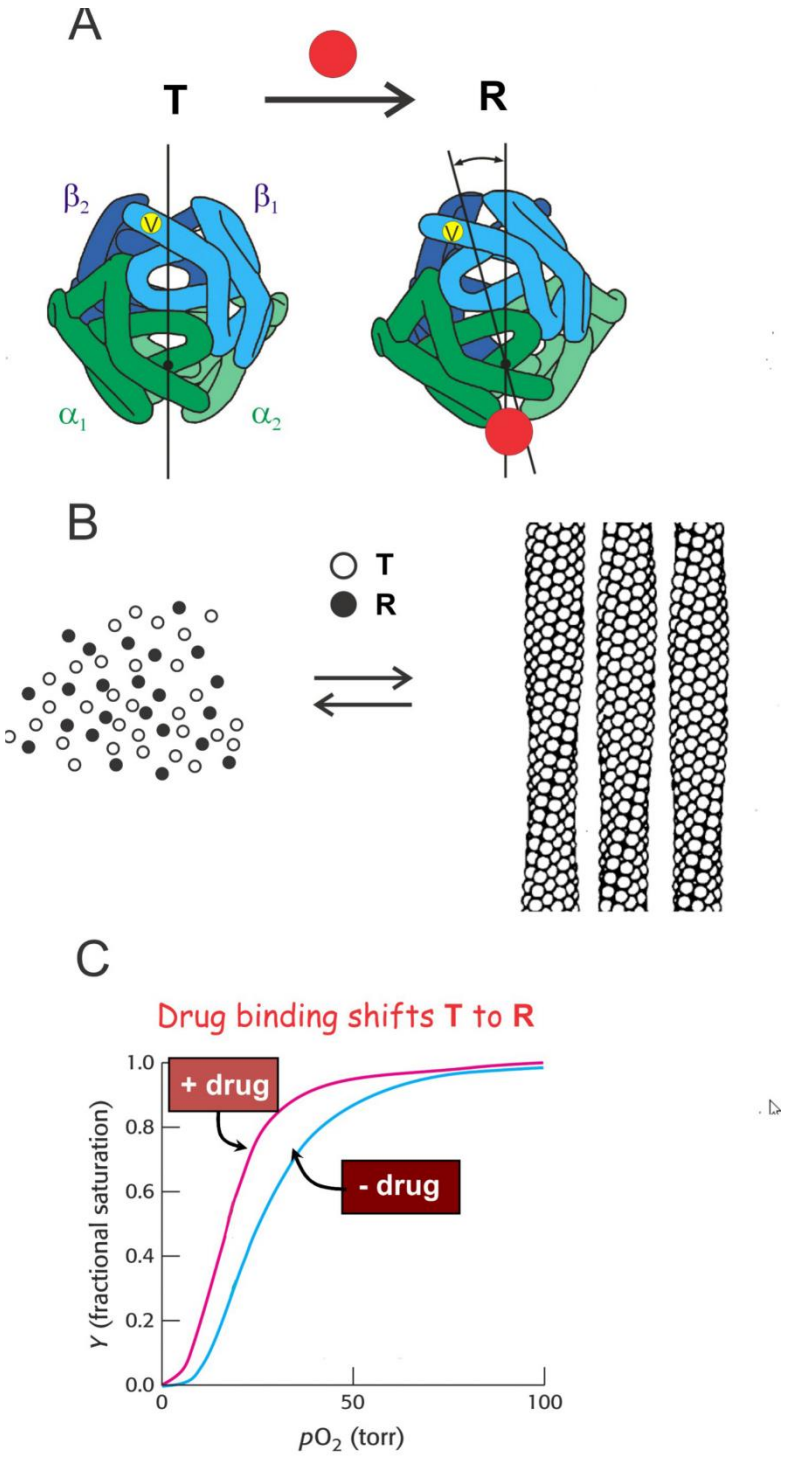

Figure IV.3. Mechanism of polymerization inhibition by increasing oxygen affinity from ref. (59)**. (**A) Hemoglobin exists in a rapidly reversible equilibrium between low and high affinity quaternary conformations, called T and R, respectively (27, 93). They differ primarily by a ~15° relative rotation of αβ dimers. Location of beta 6 valine is shown as a yellow dot on the surface of the molecule. Preferential binding of a small molecule such as a drug (red circle) to R shifts the quaternary equilibrium toward R. (B) Cartoon of polymerization equilibrium. Only the T quaternary structure (empty circles) enters the fiber. R quaternary conformations (filled circles) are completely excluded (25). (C) Oxygen binding curves. Preferential binding of a drug to the R quaternary structure causes a left shift (increased oxygen affinity).

The MWC analysis of the control of polymerization by oxygen strongly suggests that shifting the T-R equilibrium toward R, which increases the oxygen affinity, could be a sound way to inhibit

HbS polymerization *in vivo* and therefore be an effective treatment strategy. Indeed, years ago, this rationale prompted Ernest Beutler to increase the fraction of R hemoglobin in a small number of sickle cell patients by induction of either methemoglobin (94) or carboxyhemoglobin.(95) He found that either intervention resulted in a significant prolongation of red cell life span. However neither could be adapted for practical and safe long-term therapy. Current advances in drug discovery and high throughput screening offer hope of developing small molecules that bind to R preferentially and with high specificity and would therefore be a compelling therapeutic approach (96, 97). The potential downside of altering the T-R equilibrium is that the resulting "left shift" in the oxygen binding curve (Fig. 4C) could potentially decrease oxygen delivery in a disease where the patients already suffer from impaired blood flow and oxygen transport. The question, however, is what is the net effect – reduced oxygen delivery from the left shift or improved oxygen delivery from decreased sickling and therefore decreased vaso-occlusive events. The physiology is too complicated to make any predictions based on biophysical studies, but as discussed below, the results of clinical studies currently underway, should provide the answer to this question.

IVd. Reduce concentration of 2,3-diphosphoglycerate. 2,3-diphosphoglycerate (DPG) is the major allosteric effector for hemoglobin (98-100) and has three effects on HbS polymerization. It binds in the cleft between the β subunits (Fig. IV.4A,B) to stabilize the deoxy (T) quaternary structure and thereby decreases oxygen affinity by shifting the T-R quaternary equilibrium towards T (Fig. IV.4C) (101, 102). Thus, lowering DPG concentration would increase the fraction of HbS in the non-polymerizing R quaternary structure (103). A second effect of DPG is its stabilization of the fiber, as shown by a decrease in the HbS solubility.(104) Although the decrease in solubility is only ~ 10 % (104), the presence of DPG will have a dramatic effect on the kinetics of polymerization, i.e. the delay time (41), which depends on about the 30^{th} power of the solubility (41, 55, 105), Finally, lowering DPG concentration results in a third, albeit smaller, but therapeutically significant increase in solubility because of an accompanying rise in the intracellular pH (106) via the Gibbs-Donnan equilibrium. Over the physiologic intracellular pH range 7.2-7.3 the solubility of deoxy HbS increases significantly with rising pH (87). Thus, reduction of red cell DPG increases both the solubility and delay times by three independent mechanisms.

The importance of DPG in the pathophysiology of sickle cell disease is underscored by two recent and highly relevant case reports. Individuals with sickle trait (AS), which is normally a totally benign condition, have a clinical phenotype almost as severe as SS disease when they also inherit a deficiency in red cell pyruvate kinase that causes a marked elevation of red cell DPG (107, 108).

Because DPG plays such a critical role in potentiating HbS polymerization, there is compelling rationale for the development of drugs that target the enzymatic pathway responsible for its remarkably high (5 mM) concentration in red cells. A number of anions stimulate the "phosphatase" activity of DPG synthase, thereby lowering DPG levels. In particular, in the presence of 0.02 mM phosphoglycolate, the dephosphorylation of DPG is activated more than 1000-fold (109). Accordingly the addition of 30–40 mM glycolate to a suspension of normal human red cells results in a rapid decrease in DPG without any impact on ATP levels (110).

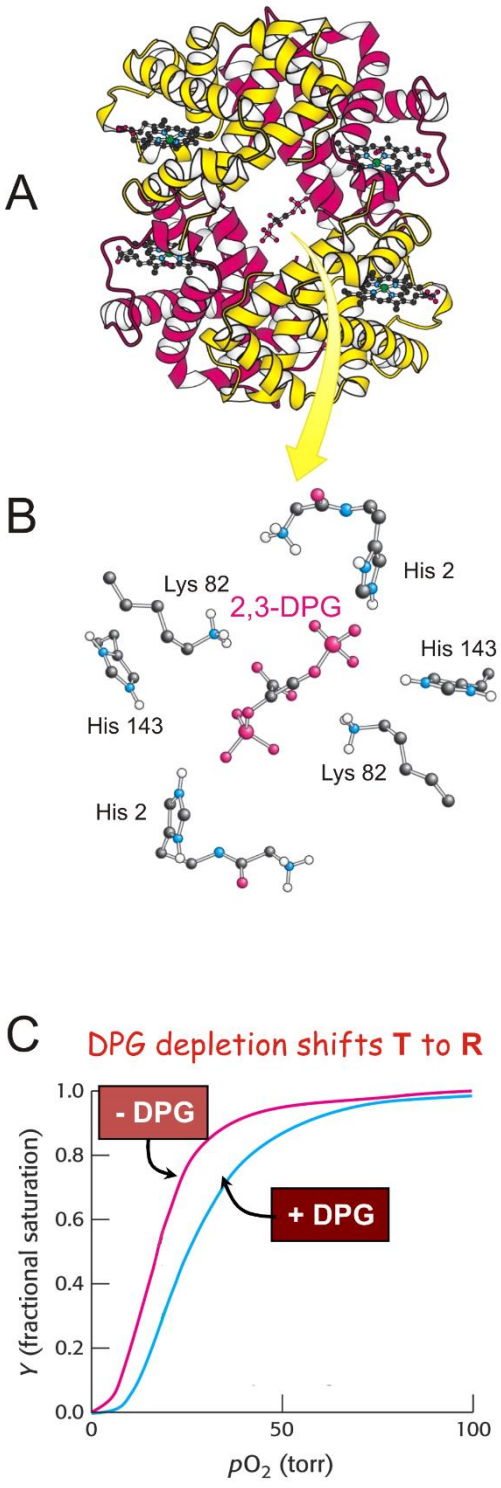

Figure IV.4. Binding of 2,3-diphosphoglycerate (DPG) to hemoglobin from ref. (59). (A and B) DPG binds in the cleft between the beta (yellow) subunits of the T quaternary structure. (C) Reduction of DPG concentration shifts the quaternary equilibrium toward R to produce a left-shift in the binding curve and increases the solubility (the concentration of Hb in the liquid phase). Both factors decrease sickling.

IVe. Reduce intracellular hemoglobin concentration. The discovery of the enormous sensitivity of the kinetics of fiber formation to HbS concentration (74, 111) led several investigators to exploit this finding in both physiological and clinical studies. The red cell behaves like a micro-

osmometer with a volume that depends on the osmolality of the plasma (112). Consequently, sensitivity of the delay time to concentration suggested that therapeutic benefit could result from an increase in red cell volume sufficient to reduce the intracellular Hb concentration by as little as 10% (49). An early unblinded, limited clinical study did in fact report that lowering of plasma osmolarity via induction of hyponatremia reduced the frequency of pain crises (113). Although maintenance of sustained low sodium diet is impractical, an important result of this study was that red cells could be swollen without serious side effects that might result from osmotic effects on other cells (113). Reduction in intracellular hemoglobin concentration is commonly encountered in patients who develop iron deficiency. In mouse models of sickle cell disease, induction of iron deficiency by suppression of intestinal expression of HIF-2α resulted in increased hemoglobin levels accompanied by reduction in MCHC and hemolytic rate (114). In SS patients who have sustained blood loss either by hemorrhage or by iatrogenic phlebotomy sufficient to result in iron deficiency, the decrease in MCHC was accompanied by increased hemoglobin and less hemolysis (115).

When red cells sickle, damage to the membrane results in calcium influx which triggers enhanced potassium efflux via the so-called Gardos channel. As a result, the red cell hemoglobin concentration increases along with a marked increase in the probability of further sickling. Therefore, inhibition of this channel is a plausible therapeutic approach. Treatment with Senicapoc (ICA-17043), a highly potent Gardos inhibitor, resulted in a decrease in red cell density and MCHC, increased hemoglobin levels and reduced hemolysis in both a sickle mouse model (116) and in sickle cell patients (117). However, a Phase 3 study was terminated early because administration of this drug appeared to cause a slight increase in the rate of sickle pain crises (118). Although the rationale for Gardos channel inhibitors is sound, like other treatment strategies under investigation, the efficacy of these drugs depends on damage to the red cell membrane caused by cycles of cell sickling and unsickling from HbS polymerization and depolymerization.

Another approach to increasing red cell volume, proposed many years ago, is to use ionophores (119). These agents transport extracellular sodium ions into the red cell, accompanied by water influx to maintain osmotic equilibrium and, in doing so, swell the red cell. A new and sensitive sickling time assay, described in Chapter 5, has shown that potentially therapeutic levels of inhibition can be achieved at sub-nanomolar concentrations of ionophores, making increase in red cell volume a viable approach to therapy (120),

Figure IV.6. Schematic of normal and swollen red cell from ref. (59). A small increase in red volume to decrease the intracellular HbS concentration dramatically increases the delay time of sickling because of its enormous dependence on the HbS concentration. Even a 10% increase in cell volume is predicted to have a therapeutic effect (49, 120).

IVf. Anti-polymerization drugs currently in clinical trials. The website www.clinicaltrials.gov lists an impressive number of recent and on-going investigations into various aspects of sickle cell disease. In a review published last year (121), Telen covered a wide range of treatments that focus on downstream sequelae of sickle vaso-occlusion, including 5 agents that target adhesion, 7 agents that target inflammation, 5 involving anticoagulants, and 6 anti-platelet agents. In contrast, Telen's review covers fewer drugs that directly target HbS polymerization. These include four drugs that induce HbF expression. However none of them currently appear to offer convincing advantages over hydroxyurea.

Among the drugs listed as an anti-sickling agent is SCD-101, a plant extract similar to Niprisan (Nix-0699). Niprisan is an ethanol-water extract from seeds, stems, fruit and leaves of four different

plants, has been used among diverse folk groups in Nigeria, and reported to be effective in lowering the frequency of pain crises in sickle cell patients (122, 123). Niprisan inhibits *in vitro* sickling and increases both the solubility and delay time of solutions of deoxyhemoglobin S, albeit in a highly non-physiological buffer (124). Moreover, the extract prolonged the survival of transgenic sickle mice following acute hypoxic challenge (125). A recent Phase 1B dose escalation study of 26 SS and S/β^o thalassemia patients found that SCD-101 was well tolerated and, at higher doses, appeared to relieve chronic pain and fatigue but had no impact on hemoglobin levels or hemolysis (126).

Telen's review (121) lists only one anti-sickling agent undergoing clinical trials that is known to directly modify hemoglobin structure: 5 hydroxymethylfurfural (Aes-103). This agent is an aldehyde that forms a reversible Schiff base linkage primarily with the N-terminal amino of α-globin resulting in a dose-dependent increase in oxygen affinity (127-129). A significant concern with aldehyde drugs is their potential to covalently modify other cellular and plasma proteins. More recently a polyaromatic aldehyde, GBT440, has been developed that also binds via a Schiff base to α-globin N-terminus with enhancement of oxygen affinity similar to Aes-103, but with higher specificity and at much lower concentrations (130). At doses that achieve an optimal increase in oxygen affinity, the partition between levels of GBT440 in the red cell and plasma is a remarkable 70:1 ratio. In initial clinical trials in normal volunteers and in sickle cell patients, once a day oral administration of GBT440 is well tolerated with no significant adverse effects (131, 132). Patients with SS disease have a dose-dependent increase in hemoglobin levels within two weeks of initiating therapy, accompanied by a decrease in reticulocyte count, serum non-conjugated bilirubin and fraction of irreversibly sickled cells in peripheral blood films (131, 132). Thus, GBT440 results in a significant prolongation of red cell life span in sickle cell patients. The crucial question, of course, is the impact of this drug on the incidence and severity of pain crises and on vaso-occlusive organ damage. The efficacy and safety of the drug is now being investigated in a double blind multi-center Phase 3 study of approximately 300 patients. The progress thus far with this drug offers a strong impetus to discover and evaluate other drugs that directly target HbS polymerization.

IVg. Conclusion. Because there are so many ways to inhibit HbS polymerization, there is cause for optimism. Of course once a polymerization inhibitor is discovered, many hurdles must be overcome, including issues of toxicity, bioavailability, pharmacokinetics, etc., before it can become an FDA-approved drug. It would therefore be prudent to first investigate the anti-polymerization effect of the numerous molecules, in addition to FDA-approved drugs, for which toxicity information exists. Major therapeutic effects could result by administering a combination of drugs, which, by acting on different molecular targets, would be non-competitive. For methods other than the promotion of HbF synthesis, drug discovery could be accelerated by carrying out screens with intact red cells, such as the recently reported laser-photolysis method for measuring sickling times of sickle trait cells (120). The Eaton lab is currently developing a technically less-demanding assay that could be used in a high throughput screen.

Chapter V

Using Kinetics to Screen Compound Libraries with High Sensitivity (120)

Va. Introduction and background. With an appropriate sibling match, sickle cell disease can be cured in both children and adults by stem cell transplantation (133, 134). Moreover, sickle cell disease is a testing ground for the exciting emerging methods of gene therapy and gene editing (135). While these are potential therapies for patients in the US, neither will be available for several decades for millions of patients in sub-Saharan Africa, India, and elsewhere (136). What is urgently needed, therefore, to treat the vast majority of patients is an affordable drug that can be taken orally. The development of hydroxyurea has been a major advance in the treatment of sickle cell disease, but is only partially effective in preventing vaso-occlusive crises (137-139).

My lab has developed a sensitive and quantitative assay that is directly connected to pathogenesis and can be used to screen for inhibition of fiber formation inside cells. Our assay is based on the highly unusual kinetics of polymerization characterized by a delay period prior to fiber formation that is enormously sensitive to the intracellular HbS concentration and on the recognition that a major determinant of clinical severity is whether the delay time is longer or shorter than the transit time thru the narrow vessels of the tissues (55, 75, 76) (Figs. I.4 and III.5). Hydroxyurea is therapeutic because it induces the synthesis of fetal hemoglobin (HbF) (138, 140), which inhibits polymerization to markedly increase delay times that allow more red cells to escape to larger vessels before fibers form (85, 141). However, hydroxyurea does not act on all cells, which reduces its efficacy (46, 142-144), so there is considerable effort to discover targets and eventually develop drugs that will alter HbF synthesis in every cell (82). The search for a drug that inhibits fiber formation in all cells, other than by altering hemoglobin synthesis, has been hampered by the lack of a screening assay that can be performed on cells. Our assay accurately and sensitively tests for inhibition of intracellular polymerization in a 96 well-plate format by measuring sickling time distributions in cells from patients with sickle cell trait, the heterozygous condition. Polymerization is induced by photodissociation of the hemoglobin-carbon monoxide complex (HbCO) with a continuous wave (cw) laser to rapidly create and maintain hemoglobin in the deoxy form that aggregates to form fibers. Fibers are detected by alterations in red cell morphology using a unique and robust image analysis algorithm. Using this assay, we have discovered powerful polymerization inhibitors that act by producing small increases in cell volume to decrease the intracellular hemoglobin concentration, indicating that increasing cell volume is a viable approach to therapy.

Rationale for screening with sickle trait cells. The use of cells addresses the very important question of penetration of the red cell membrane by a potential drug. It also allows the detection of drugs that increase sickling times by several different methods, including decreasing the intracellular hemoglobin concentration by increasing cell volume, blocking inter-molecular contacts in the fiber, or weakening contacts, for example, by increasing intracellular pH (105) or by decreasing 2,3-diphosphoglycerate synthesis (104). There are many advantages to using cells from donors with sickle cell trait (AS), the heterozygous condition, rather than cells from patients with homozygous sickle cell (SS) disease. (i) Sickle trait is a benign condition and far more prevalent (~8% of African Americans) than sickle cell disease, so that blood samples are much more readily available. Moreover, many sickle trait patients have relatives with sickle cell disease, so they are more than willing to donate blood

samples as frequently as requested. The sickle trait cell population is much more homogeneous and therefore the interpretation of results is more straightforward. The cell population is more homogeneous because trait cells sickle very much less frequently *in vivo* and so incur relatively little or no damage compared to SS cells, which undergo many sickling/unsickling cycles (75, 145). The large dilution of HbS by normal hemoglobin (HbA) in trait cells increases the sickling time by several orders of magnitude without changing the mechanism of fiber formation (12, 49, 91, 146, 147). Even though there is less fiber formation in sickle trait cells, the longer delay times produce larger distortions than observed for deoxygenated SS cells, making it easier for image analysis to accurately determine sickling times. Larger distortions occur because there are fewer homogeneously-nucleated fibers and therefore fewer domains of fibers (148). The longer sickling times (146) compared to SS cells (51, 141) also allow a much lower laser power density to achieve complete photodissociation of the HbCO complex. With the lower power density a defocused laser beam and larger field of view can be used for simultaneous observation of many cells (up to 200) compared to one cell at a time in previous photolysis experiments with SS cells (51, 141).

Sample preparation and measurement of sickling times. The main consideration in preparing samples is to obtain cells with hemoglobin as the CO complex in a near physiological buffer in a 96-well plate at 37^{o}C in the complete absence of oxygen. CO is used instead of oxygen because the HbCO complex is much more readily photodissociated than the oxygen complex. All oxygen must be eliminated because it would bind to hemoglobin very rapidly and artifactually increase the sickling time. The procedure consists of adding the candidate drug to wells containing a dilute suspension of CO-saturated sickle trait cells, sealing the well plate to prevent loss of CO, placing the plate in a 37^{o}C incubator purged with humidified nitrogen for either 4 or 24 hrs, unsealing the well plate under a nitrogen atmosphere, and adding sodium dithionite to remove any traces of oxygen. The well-plate is then resealed and transferred to the microscope and mounted on an *xy* translation stage for well-by-well sickling time measurements at 37^{o}C.

Fiber formation is induced by photodissociating the CO from hemoglobin with a cw argon ion laser operating at 514 nm to rapidly (~0.2 sec) form and maintain close to 100% deoxyhemoglobin. Following photolysis images of the cells are collected on a CCD camera at 100 ms intervals for 60 sec, which is sufficiently long to sickle more than ~60% of cells, which contain a ~60/40 HbA/HbS mixture. A complete well-plate experiment consists of a sequence of such photolysis experiments performed on the wells in a specified order. The entire experiment is performed under computer control using LABVIEW (National Instruments). This software controls the sequence in which the wells are imaged by moving an *xy* stage on which the well plate is mounted, as well as the gating of laser illumination and the input and storage of the set of camera images for each well.

Although nitrogen is flowed over the sealed well plate, we have not been able to find a transparent material that makes a seal that is completely impermeable to oxygen. Consequently, the duration of the sickling time measurements for 96 wells is limited to 3-4 hours because of eventual oxygen leaks.

Details of sample preparation. 2 ml heparinized blood samples were obtained at the NIH clinical center phlebotomy unit from anonymized sickle trait donors under NIH protocol 08-DK-0004. The hemoglobin was converted to the CO form and the blood diluted 3000-fold into pH 7.4, 305 mOsM (determined by freezing point depression osmometry), nitrogen-deoxygenated buffer containing 10 mM sodium chloride, 32 mM disodium hydrogen phosphate, 8 mM potassium dihydrogen phosphate, 5.5 mM dextrose, and 1 g/l bovine serum albumin. The cell suspension was gently stirred under a CO

atmosphere for 45 minutes. Using an 8-channel pipette, 50 μl aliquots of the cell suspension were dispensed into wells of a clear polystyrene base 96-well plate (Greiner Bio-One) under a nitrogen atmosphere. 5 μl aliquots of drugs at various concentrations in the same buffer were then added to each well and the plates sealed with aluminum foil, After incubating at 37°C in a nitrogen flow incubator (Thermo Scientific) for 4 or 24 hrs, the plates were placed in a room-temperature nitrogen box, unsealed, and 50 μl of a 10 mM freshly prepared sodium dithionite solution in CO saturated buffer (pH 7.2, 30 mM disodium hydrogen phosphate, 10 mM potassium dihydrogen phosphate, 5.5 mM dextrose, 1 g/l bovine serum albumin) was added to each well to remove any traces of oxygen. The final pH and osmolarity were 7.3 and 305 mOsM. The plates were resealed with a transparent polypropylene film (Greiner Bio-One) and kept at 37°C for 45 minutes before starting the sickling time measurements. Strict anaerobiosis during the sickling time measurements could only be maintained for up to about 4 hours, making it impractical to collect images from each well for longer than 60 seconds.

The sources and purity for inhibitors are: gramicidin A (Sigma, >90% purity), monensin A (Calbiochem, >97.5% purity), 5-hydroxymethyl-2-furfural (Sigma-Aldrich, >99% purity), and 2-hydroxy-6 ((2-(1-isopropyl-1H-pyrazol-5-yl) pyridin-3-yl) methoxy) benzaldehyde) (synthesized by Chem-Master International, >97% purity).

Determination of sickling time distribution from images. Pictures of 100-200 cells on the bottom surface of the well plate are digitized as a series of 8-bit grayscale, 1280 X 960 pixel images (Fig. V.1) and saved as JPEG files. To establish grayscale ranges, analysis is first conducted on images at 0.1 sec post-photolysis, when hemoglobin is almost completely in the deoxy form and no cells have sickled. Pixel values for all images are transformed to maximize the dynamic range of the values, followed by assigning each pixel to either a cell or background (see S.I. for details). Based on this classification, a list of cells, defined as contiguous regions of pixels of density above a background threshold, is compiled. Regions too small to represent a red cell are removed, as are regions too large to be processed, such as two or more individual cells that overlap.. The set of pixels assigned to each remaining cell (>90%) of the list of possible cells) is tracked, which allows cells to be monitored even if they move during the 65 second observation period.

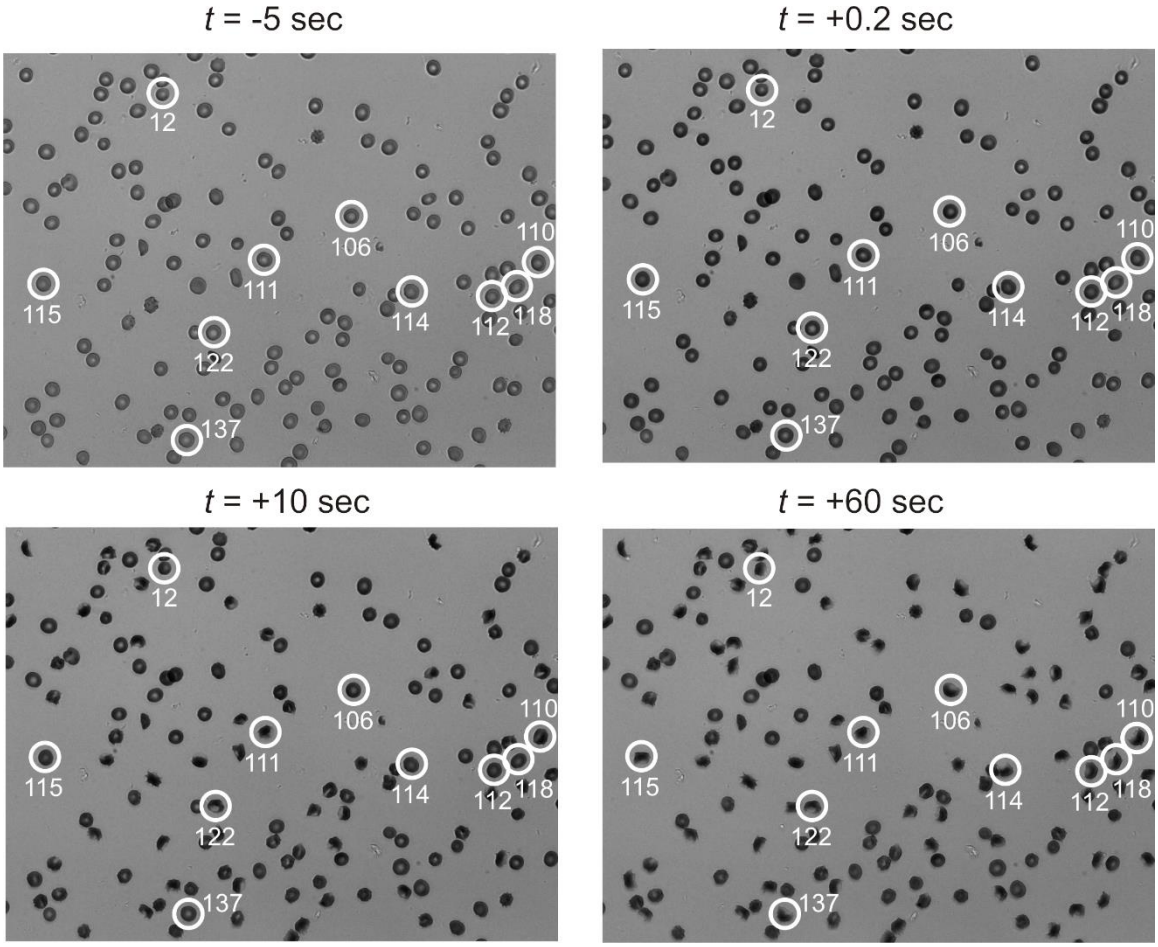

Figure V.1. Representative images of red cells prior to photolysis (-5 sec) and at 0.2 sec, 10 sec, and 60 sec post-photolysis from ref. (120). The contrast is less at -1.6 sec because the absorption maximum of HbCO is 419 nm, while that of deoxy Hb is 430 nm, which corresponds to the wavelength of maximum transmission of the band pass filter. At 0.2 sec no cells have sickled; 50% are sickled at +10 sec, and 71% are sickled at 60 sec. Data from the analysis of the cells circled in white is shown in Figure V.2.

The determination of the sickling time is based on the reasoning that fiber formation is the only possible cause of even the slightest cellular distortion. Moreover, previous studies on laser-photolysis-induced polymerization showed that distortion of SS cells is simultaneous with the onset of increased light scattering (42). Three metrics describing cell morphology are computed for all 650 images of each cell before and after the start of laser illumination. These are the projected area of the cell (the number of pixels assigned to a cell), the ratio of the density on the periphery of the cell to the center (unsickled cells are biconcave discs, which are more transparent in the center, Figs. V.1 and V.2), and the deviation from a circular shape as determined by the eccentricity (the ratio of the longest to the shortest dimension of the cell). The time at which there are simultaneous changes in at least 2 of these 3 metrics is taken as the sickling time, which can be precisely determined as shown in Figure V.2A. There is a wide distribution of sickling times (Figs. V.2Bb and V.3) caused primarily by the relatively small variation in intracellular hemoglobin concentration. The experimental result, then, for each well is the fraction of cells sickled as a function of time, i.e. the cumulant of this distribution (Fig. V.2C). Also shown in Figure V.2C is the cumulant calculated from the intracellular concentration distribution and the solubility of mixtures of HbA and HbS, as described in Chapter III, except the desaturation time is 200 ms and the final saturation with CO is zero.. The excellent agreement with the experimental result indicates that there is little or no difference between polymerization in cells and in solutions of purified hemoglobins.

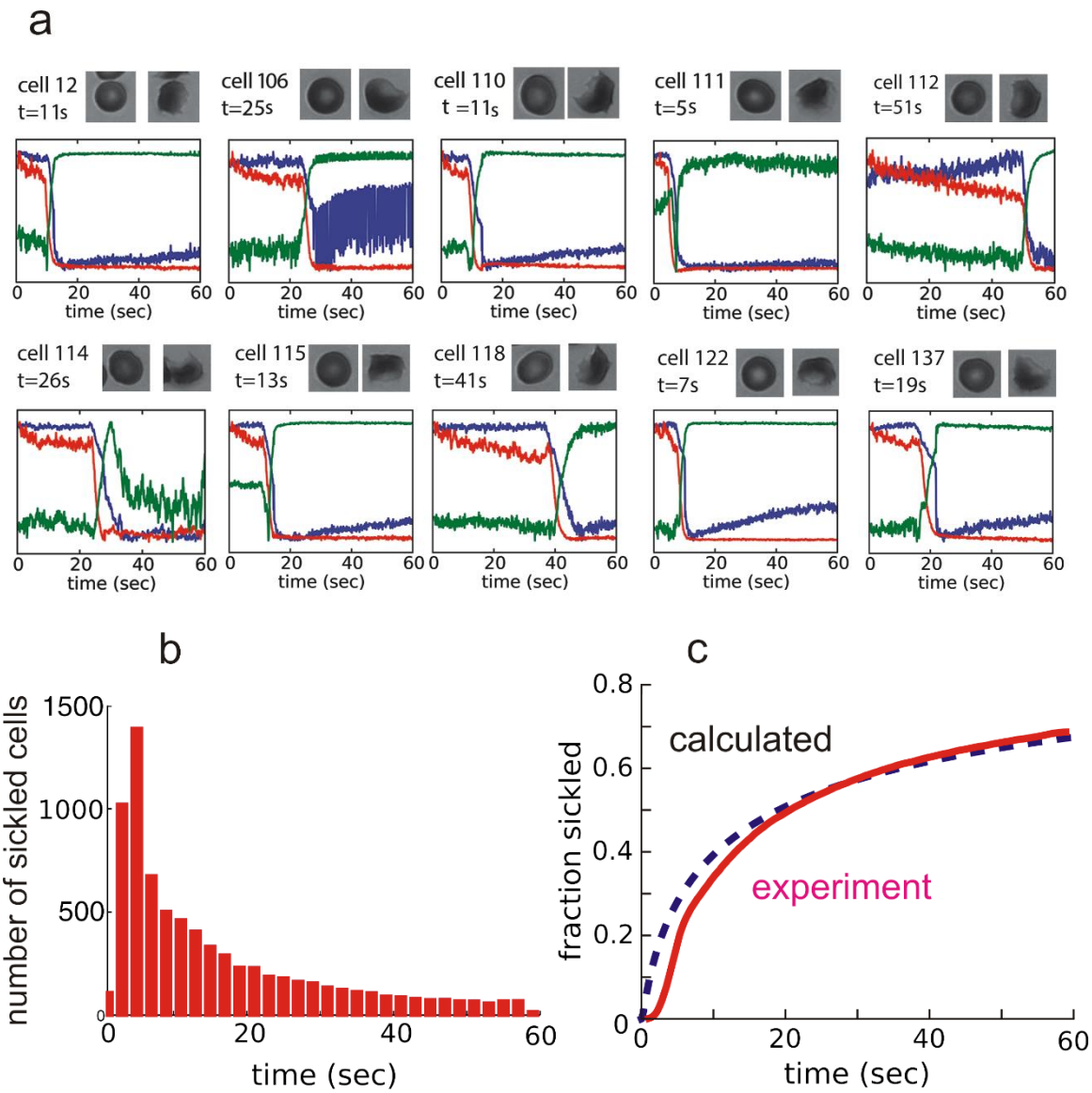

Figure V.2. Kinetic progress curves and sickling time distributions from ref.(120). (a) Images of single red cells from a trait donor before photolysis and at 60 sec. post-photolysis with curves corresponding to the 3 metrics used to detect cell distortion - area (blue), density ratio (red), and eccentricity (green). The curves were scaled so that the highest and lowest amplitudes were taken as one and zero. The noise reflects the absolute amplitudes. Analysis of photolysis experiments on CO-saturated red cells from an AA donor showed zero fraction sickled at all times up to 60 s. (b) Distribution of sickling times for ~21,000 cells from 96 wells. (c) Cumulant of distribution (red curve). The dark blue dashed curve in (c) was calculated from the universal curve of delay time versus supersaturation (the initial activity divided by the equilibrium activity) (41), using the concentration distribution for normal cells of Lew *et al.* (38) multiplied by a factor of 1.03, activity coefficients calculated from equation (S2) (Fig. S3), and solubilities at each concentration of the concentration distribution from equation (S1) using a hemoglobin composition of 38% HbS and 62% HbA (the composition for this patient is 38%HbS, 58% HbA, 3.7% HbA_2, and 0.3% HbF). Importantly, it is assumed that every cell has the same hemoglobin composition

Criteria for therapeutic inhibition. A relatively unique feature of sickle cell disease is that it is possible to take advantage of our understanding of the kinetics and thermodynamics of fiber formation and the known correlation between clinical severity and red cell composition to predict the potential

therapeutic effect from the measured increases in sickling times in our assay (12, 48, 49, 76). Previous analyses (48, 49) did not consider the distribution of intracellular concentrations and solubilites, which produces a very large distribution of sickling times for cells having the same hemoglobin composition. The longer delay times in trait cells compared to SS cells result in greater sensitivity to changes in intracellular concentration and composition. Consequently, our problem is to relate the inhibitory effects in trait cells to those in SS cells. The key to making this connection is the recent discovery of a universal relation between the delay time and the supersaturation (41) for purified hemoglobin solutions, which allows us to calculate the delay time at any concentration or solubility (see Appendix C).

Two sickle syndromes are particularly useful for our analysis. One is sickle cell disease with pancellular hereditary persistence of fetal hemoglobin (S/HPHF), in which all cells contain about 30% HbF and 70% HbS (46). Patients with S/HPHF "have symptoms of neither sickle cell disease nor hemolytic anemia" (46). A drug that increases sickling times in trait cells comparable to that expected for cells in which 30% of the HbS/HbA mixture has been replaced by HbF is therefore regarded as 'potentially curative'. The second is hemoglobin SC disease. SC cells contain 50% HbS and 50% HbC, which has the same effect on fiber formation as HbA (149). In addition to containing a higher fraction of HbS than trait cells, SC cells have a greater total Hb concentration, explaining why it is a severe sickle syndrome, albeit less severe than homozygous SS disease (149, 150). A drug that increases sickling times in trait cells comparable to that expected for cells in which 50% of the HbS/HbA mixture has been replaced by HbA (= HbC) and the intracellular concentrations increased by 10%, is regarded as 'potentially therapeutic'. From these calculations (Fig. V.3) (see Appendix D), we conclude that compounds for which no sickling occurs at 60 s are potentially curative, while compounds for which the percent sickled is 30% relative to the control (absence of the compound) are potentially therapeutic. Given the uncertainties in the calculation, in the subsequent discussion we shall regard 10% sickling at 60 s, compared to the control with no drug, as potentially curative and 60% as potentially therapeutic. Despite the fact that the calculations are only approximate, they serve as an extremely useful guide for assessing therapeutic potential. (There are, of course, many additional factors to be considered for evaluating therapeutic efficacy, including toxicity, binding to plasma proteins, pharmacokinetics, bioavailability, etc.)

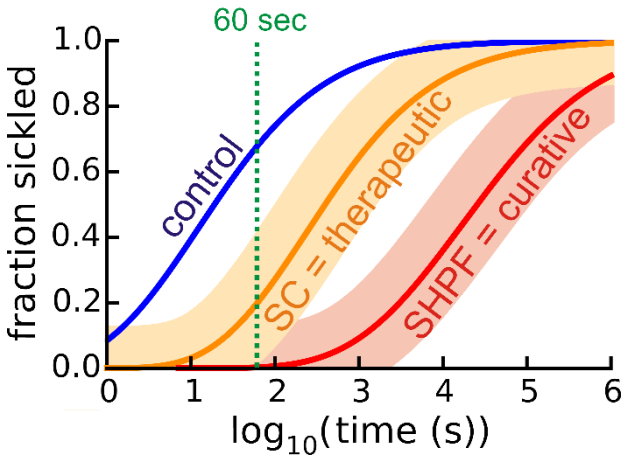

Figure V.3. Calculations of fraction sickled versus time in sickle trait cells corresponding to a predicted therapeutic effect from ref. (120). The plot shows the calculated fraction of trait cells sickled versus time after

laser photodissociation of CO. Control (blue curve): calculated as for Fig. V.2C using a composition of 38% HbS and 62% HbA. Orange curve: level of inhibition predicted to be potentially therapeutic and corresponds to the sickling times in trait cells comparable to the sickling times in cells from patients with SC disease compared to homozygous SS disease cells. Red curve: level of inhibition predicted to be potentially curative and corresponds to sickling times in trait cells comparable to the sickling times in cells from patients with sickle cell disease and pancellular hereditary persistence of fetal hemoglobin (SHPF) compared to homozygous SS disease cells. Orange and red curves calculated as in Appendix D. The shaded areas represent the uncertainties in the calculation.

Discovery of powerful inhibitors that increase red cell volume. Because there is a large amount of hemoglobin (almost 1 lb) in the average adult sickle cell patient, the amount of drug that acts by non-covalent binding to sickle hemoglobin is expected to be intolerably large. On the other hand, decreasing the intracellular hemoglobin concentration by increasing cell volume using compounds that bind to the red cell membrane should require much less. One such class of compounds is ionophores that were suggested many years ago (119). We therefore first carried out a simple and relatively high throughput pre-screen of the 1600-compound "Pharmakon Collection" (Microsource Discovery Systems), which contains a large number of clinically-tested compounds, to search for compounds that sphere red cells. Sphered red cells are easily detected because they have a smaller diameter and an increased density at the center of the cell compared to normal biconcave discs. Compounds that sphere cells are those that are also expected to increase cell volume at sub-sphering concentrations. The volume of sphered cells is approximately 1.7-fold larger than a biconcave disc. This increase in the cell volume reduces the intracellular hemoglobin concentration of all trait cells to less than 0.23 g/ml, so they will never sickle because the supersaturation is less than 1.0 or the supersaturation is so low that sickling will take much longer than 60 sec; sphered cells were never observed to change shape (i.e. sickle) at 60 sec following laser photolysis.

Two compounds that swell cells and are powerful inhibitors at sub-sphering concentrations have been discovered so far - the ionophores gramicidin A and monensin A (Figure V.4). Both compounds show inhibition that increases with incubation time. After a 4 hour incubation monensin has no therapeutically significant effect on sickling times at concentrations less than ~6 nM (Figure V.4, lower panel), while after a 24 hr incubation, threshold inhibition is observed at ~2 nM and at 6 nM achieves a level of inhibition expected for a potentially curative drug (Fig. V.3). As expected from the sphering pre-screen, monensin acts by increasing cell volume (Figure V.4, upper panel), indicating that dilution of intracellular hemoglobin is the inhibitory mechanism. In previous studies of the effect of monensin on cell volume and other cellular properties, not including sickling, concentrations less than 10 nM were not employed (119).

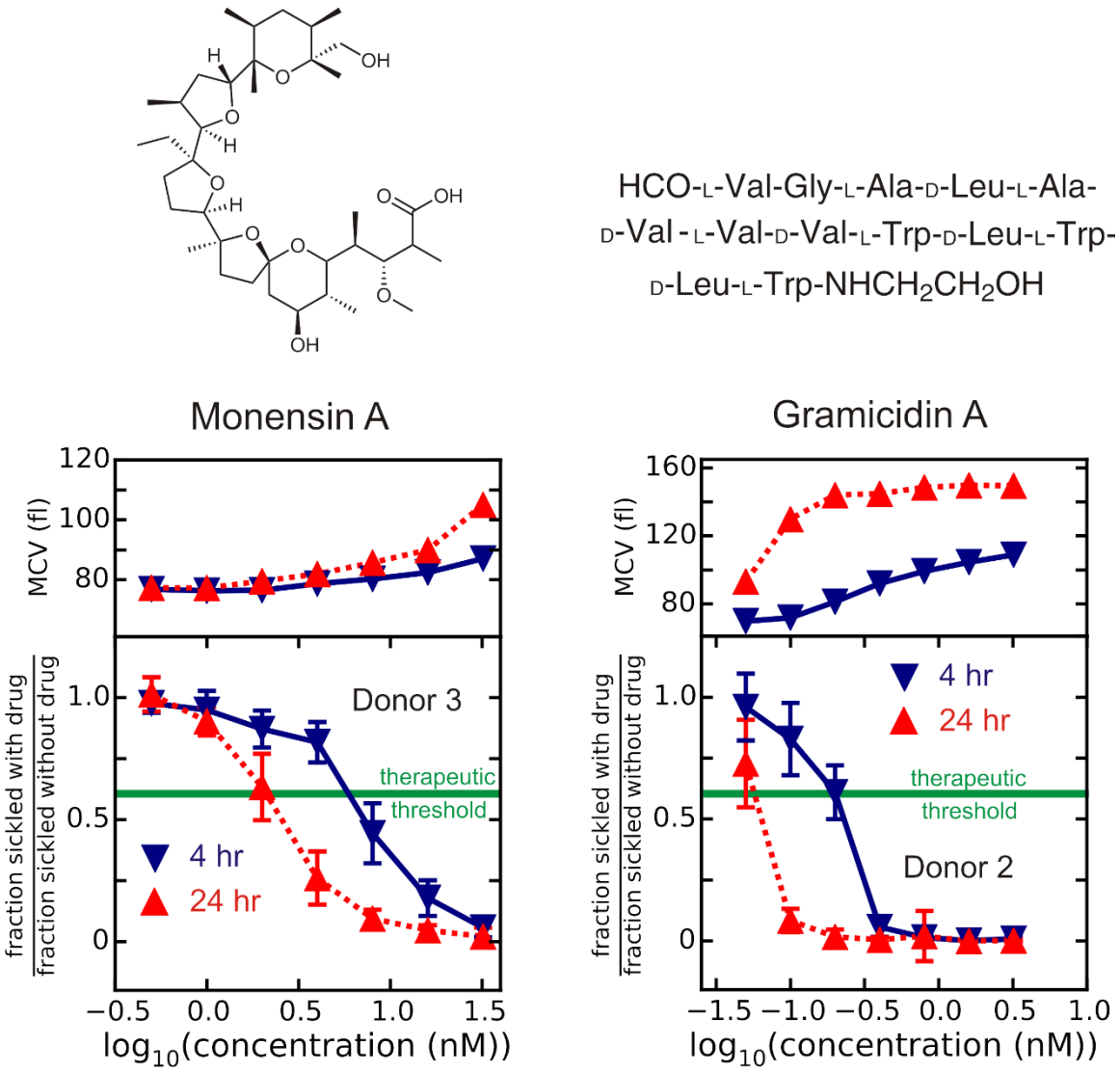

Figure V.4. Mean volume and fraction sickled at 60 sec for compounds that decrease intracellular hemoglobin concentration by swelling cells from ref. (120). Top panels: mean corpuscular volume measured with Coulter counter. Bottom panels: Fraction sickled at 60 sec post-photolysis. Blue inverted triangles are for 4 hr incubations, while red upright triangles are for 24 hr incubations. The green horizontal line is our estimate of the minimum level of inhibition required for a therapeutic effect. The error bars represent one standard deviation from the mean of 12 determinations, i.e. the fraction sickled for each of 12 wells at a single candidate-drug concentration relative to the average fraction sickle for the 12 wells of the control (no drug) in each of 12 wells, where both the mean and the standard deviation were weighted by the number of cells in the image collected from each well. There are no errors shown for the MCV, since the ratio of the standard deviation to the mean of 5 determinations is less than 1%.

Gramicidin A also acts by slowly increasing cell volume, but produces larger volume increases and correspondingly longer sickling times at much lower concentrations (Figure V.4, lower panel). Inhibition comparable to our therapeutically-significant threshold of 60% sickled compared to control is observed after 4 hrs at concentrations as low as ~200 pM and almost no sickling is observed at 60 sec at 800 pM, corresponding to a potentially curative drug (Fig. V.3). After 24 hrs of incubation at 100 pM, there only 10% sickling at 60 sec. As expected from the sphering pre-screen, gramicidin A increases cell volume (Figure V.4, upper panel), again indicating that dilution of intracellular hemoglobin is the inhibitory mechanism.

A potential seriously toxic side effect of compounds that increase cell volume is hemolysis.

However, no significant hemolysis was observed at the inhibitory concentrations, i.e. less than 10 nM for monensin and less than 800 pM for gramicidin. Ionophores are currently being tested in transgenic sickle mice to determine whether a therapeutic effect can be achieved.

Appendix A. Derivation of equation (7) for solubility of mixtures as a function of fractional saturation of hemoglobin with oxygen in the liquid phase.

The fundamental copolymerization equations of Minton for mixtures of HbS with non-S hemoglobins, including the water activity term required by the Gibbs-Duhem relation, are

$$\frac{\gamma_s c_s}{\gamma_s^0 c_s^0}\left(\frac{a_{H_2O}}{a_{H_2O}^0}\right)^n = \frac{1}{\sum x_i e_i} \qquad \text{(A1)}$$

and

$$f_i = \frac{x_i e_i}{\sum x_i e_i} \qquad \text{(A2)}$$

where c_s is the solubility, defined as the total concentration of the Hb's in the supernatant after sedimenting the fibers in an ultracentrifuge, c_s^0 is the solubility of pure HbS, the γ's are the corresponding activity coefficients, x_i is the mole fraction of species in the liquid phase (i.e. the supernatant), e_i is the copolymerization probability of tetramer i, and f_i is the fraction of tetramer i in the fiber phase. e_1 is the copolymerization probability for $\alpha_2\beta_2^S$; e_2 is the copolymerization probability for $\alpha_2\beta^S\beta^A$ or $\alpha_2\beta^S\gamma$; e_3 is the copolymerization probability for $\alpha_2\beta^A{}_2$ or $\alpha_2\gamma_2$. At every oxygen pressure, the fraction of molecules in the T quaternary structure for all three tetramers are identical, which results in the double summation (eqn. III.27 of ref. (12)). According to the MWC model, the co-polymerization probability of all T-state species, no matter the number of ligands bound, is 1.0. Equation (S1) becomes:

$$\frac{\Gamma c_s}{c_s^0} = = \frac{1}{\sum_{j=1}^{3} x_j e_j \sum_{i=0}^{4} x_{T_i}} \quad , \quad \Gamma \equiv \frac{\gamma_s}{\gamma_s^0}\left(\frac{a_{H_2O}}{a_{H_2O}^0}\right)^n \qquad \text{(A3)}$$

From the MWC partition function:

$$\frac{\Gamma c_s}{c_s^0} = \frac{1}{\sum_{j=1}^{3} x_j e_j \sum_{i=0}^{4} x_{T_i}} = \frac{1}{\sum_{j=1}^{3} x_j e_j \left(\frac{L\left(1+K_T\right)^4}{L\left(1+K_T\right)^4 + \left(1+K_R\right)^4}\right)} \qquad \text{(A4)}$$

According to the TTS model, the copolymerization probability depends on the number of ligands bound to the T-state, and equation (S3) becomes

$$\frac{\Gamma c_s}{c_s^0} = = \frac{1}{\sum_{j=1}^{3} x_j e_j \sum_{i=0}^{4} x_{T_i} \left(\frac{K_P}{K_T} \right)^i} = \frac{1}{Z \sum_{j=1}^{3} x_j e_j} \qquad \text{(A5)}$$

$$Z \equiv \frac{L\left(1+K_P p\right)^4}{L\left(1+K_T p\right)^4 + \left(1+K_R p\right)^4}$$

and

$$f_i = \frac{Z c_s x_i e_i}{\Gamma c_s^0} \qquad \text{(A6)}$$

Conservation of mass for each tetrameric species *i* requires:

$$f_i x_p + x_i \left(1 - x_p\right) = X_i \qquad \text{(A7)}$$

where the fraction polymerize is:

$$x_P = \frac{1 - c_s / c_0}{1 - c_s / c_P} = \frac{c_P \left(c_0 - c_s\right)}{c_0 \left(c_P - c_s\right)} \qquad \text{(A8)}$$

Replacing x_P in eqn. (S) by eqn (S8) results in

$$f_i c_P \left(c_0 - c_s\right) + x_i c_s \left(c_P - c_0\right) = X_i c_0 \left(c_P - c_s\right) \qquad \text{(A9)}$$

Substituting for x_i from eqn. (6) gives

$$f_i c_P \left(c_0 - c_s\right) + \frac{f_i \Gamma c_s^0}{Z c_s e_i} c_s \left(c_P - c_0\right) = X_i c_0 \left(c_P - c_s\right) \qquad \text{(A10)}$$

For the homotetramer $\alpha_2\beta_2^S$ $e_1 = 1$, and equation (10) becomes

$$\begin{aligned} f_1 \left[c_P Z c_s \left(c_0 - c_s\right) + \Gamma c_s^0 c_s \left(c_P - c_0\right) \right] \\ = \left(1 - X_A\right)^2 Z c_s c_0 \left(c_P - c_s\right) \end{aligned} \qquad \text{(A11)}$$

For the hybrid tetramer $\alpha_2\beta^S\beta^A$, $e_2 \neq 0$, and the mass conservation equation is

$$\begin{aligned} f_2 \left[Z c_s e_2 c_P \left(c_0 - c_s\right) + \Gamma c_s^0 c_s \left(c_P - c_0\right) \right] \\ = \left[2 X_A \left(1 - X_A\right) \right] Z c_s e_2 c_0 \left(c_P - c_s\right) \end{aligned} \qquad \text{(A12)}$$

Since $e_3 = 0$ for the homotetramers $\alpha_2\beta^A{}_2$ and $\alpha_2\gamma_2$, $f_2 = (1\text{-}f_1)$. Therefore, replacing f_2 with $(1\text{-}f_1)$ from eqn. S(11) gives the final working equation:

$$\left[ZB_1 + B_2 - (1-X_A)^2 ZB_3 \right]\left[Ze_2 B_1 + B_2 \right] - \left[2X_A(1-X_A) \right]\left[ZB_1 + B_2 \right] Ze_2 B_3 = 0 \qquad \text{(A13)}$$

$$B_1 \equiv c_P(c_0 - c_s),\ B_2 \equiv \Gamma c_s^0 (c_P - c_0),\ B_3 \equiv c_0(c_P - c_s)$$

Appendix B. Derivation of Szabo equation for calculating sickling times.

When the homogeneous nucleation rate is small compared to the heterogeneous nucleation rate, as is the case for the delay times comparable to the ~ 1 sec transit time of red cells through the microcirculation, the concentration of polymerized hemoglobin (Δ) exponentially (12, 92), i.e.

$$\Delta(t) = \frac{1}{2} A \exp(Bt) \qquad \text{(A14)}$$

Equating the delay time (t_d) to the tenth time ($t_{1/10}$), i.e. the time at which one-tenth the concentration of polymerized hemoglobin that is formed at equilibrium (Δ(4)), the delay time is given by (12, 92)

$$t_d = t_{1/10} = \frac{1}{B} \ln\left(\frac{\Delta(\infty)}{5A} \right) = \frac{C}{B}, \qquad \text{(A15)}$$

where the constant C is $\ln(\Delta(\infty)/5A)$. As the saturation of HbS with oxygen decreases with time, the delay time also decreases. Treating the parameter B as a time-dependent rate coefficient and the parameter A as time-independent because of the much lower sensitivity of the delay time to A, the concentration of polymerized hemoglobin is now given by

$$\Delta(t) = \frac{1}{2} A \exp\left(\int_0^t B(\tau) d\tau \right) \qquad \text{(A16)}$$

The concentration of polymerized hemoglobin is ~Δ(4)/10, when the upper limit of the integral is the delay time for the cell, i.e. the sickling time

$$\int_0^{t_{sickle}} B(\tau) d\tau = C \qquad \text{(A18)}$$

Substituting $\frac{C}{t_d(t)}$ for $B(t)$ from eqn. (S15),

$$\int_0^{t_{sickle}} \frac{d\tau}{t_d(\tau)} = 1 \qquad \text{(A19)}$$

which shows that, knowing the time dependence of the delay time, the sickling time (t_{sickle}) is given by the time at which the integral = 1.

Appendix C. Universal relation between delay time and activity supersaturation (41).

The results of a review of all of the published delay time and solubility data (91, 92, 105, 147, 149, 151-153) are shown in Figure A1. Because the solutions are extremely non-ideal due to large excluded volume effects at the high protein concentrations of the experiments, called "macromolecular crowding", the thermodynamically effective concentrations are not the measured concentrations, but

are activities obtained by multiplying the concentration by the known activity coefficient (24). In the concentration range of the experiments from 0.16 g/ml to 0.4 g/ml discussed here, the corresponding activity coefficients are 4 to 200 (see equation 2 of main text), so non-ideality plays a very important role in determining the thermodynamic driving force for this reaction.

Figure A1 shows that that there is no correlation of the delay time with fiber stability and only a weak correlation with the initial protein concentration. There is, however, a striking collapse of all the data onto a single universal curve when the delay time is plotted versus the supersaturation, which is the ratio of the initial protein concentration to the solubility, expressed as activities (Fig. S1) (41).

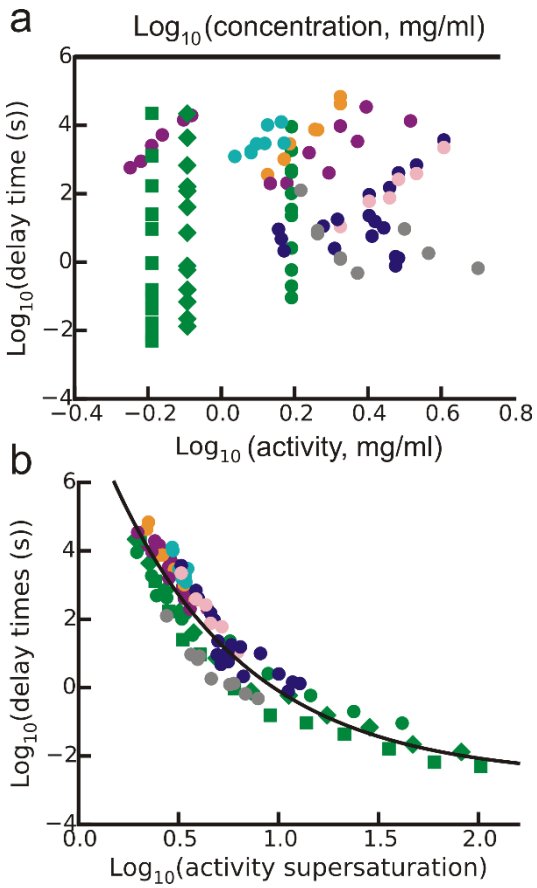

Fig. A1. Universal relation between delay time and supersaturation from ref. (41). (a) Delay time versus solubility (the concentration of HbS in the liquid supernatant after fibers are sedimented) and the activity (supernatant concentration multiplied by activity coefficient from equation (2). Unlike most chemical reactions for which the rate increases as the stability of the products relative to the reactants increases (linear free energy relations), there is no correlation at all between the delay time and the stability of the fiber as determined from the solubility. (b) However, when the delay time is plotted versus the ratio of the initial activity prior to fiber formation to the activity in the liquid phase (the supernatant), the data collapse onto a single universal curve, no matter how the solubility is varied (changes in temperature, carbon monoxide concentration, dilution of HbS with non-S hemoglobins, etc) (41). The continuous curve ($y = a \exp(-bx) + c$) is a least-squares fit to the data, where y is $\log_{10}$(delay time), x is the activity supersaturation, a = 11.2 ∀ 0.5, b = 1.49 ∀ 0.20, c = -2.64 ∀ 0.48. For very low supersaturations, an additional term would be required to ensure that the delay time approaches infinity at a supersaturation of 1.0 (x = 0). The r.m.s. deviation of the experimental delay times from the empirical universal curve is 0.65.

Appendix D: Calculation of fraction sickled vs time:

The calculation is done in several steps.

(1) Calculate the fractional saturation of HbS as a function of time from equation (3) for a given exponential decrease in oxygen pressure to a given final pressure assuming instantaneous attainment of the equilibrium saturation with oxygen at each pressure.

(2) At each time point, calculate the solubility of HbS from the solubility line in Figures 4, 6 or 7 of main text.

(3) At each time point, calculate the supersaturation ratio for each cell with an intracellular concentration distribution from the distribution in Figure 5 of main text.

(4) At each time point, calculate the delay time for each cell using the universal curve of Figure S1 above to yield a delay time.

(5) At each time point, evaluate the integral in equation 8 for each cell. When the integral equals unity, a sickling time is assigned to that cell.

(6) Repeat steps 1-5 for each cell to determine the distribution of sickling times from the distribution of intracellular concentrations in Figure 5.

(7) Calculate the fraction sickled as a function of time from the distribution of sickling times obtained in step 6.

The results for each step of the calculation for the concentration distributions in Fig 5. and the solubilities of Figs 4,6, and 7 of the main text are shown in Figs. A2, A3, and A4.

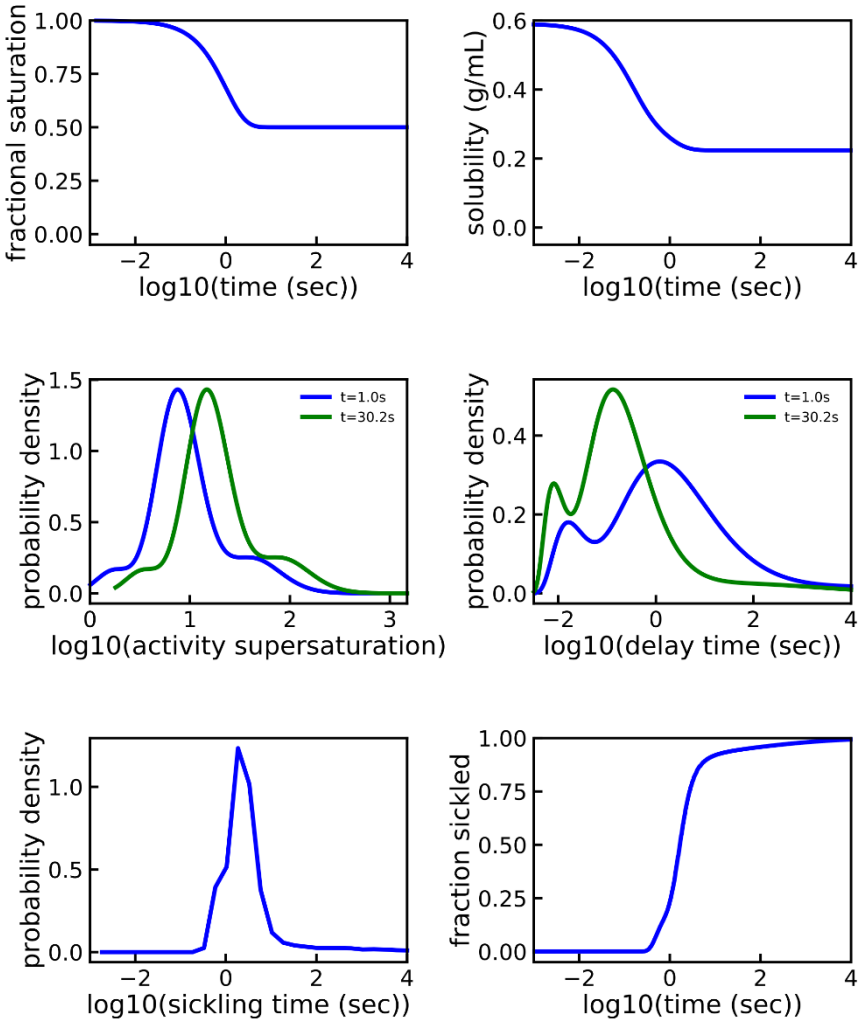

Figure A2: 6 steps in calculation of fraction sickled vs time for 1 sec desaturation to 50% saturated for concentration distribution of Bartolucci patient SS3.

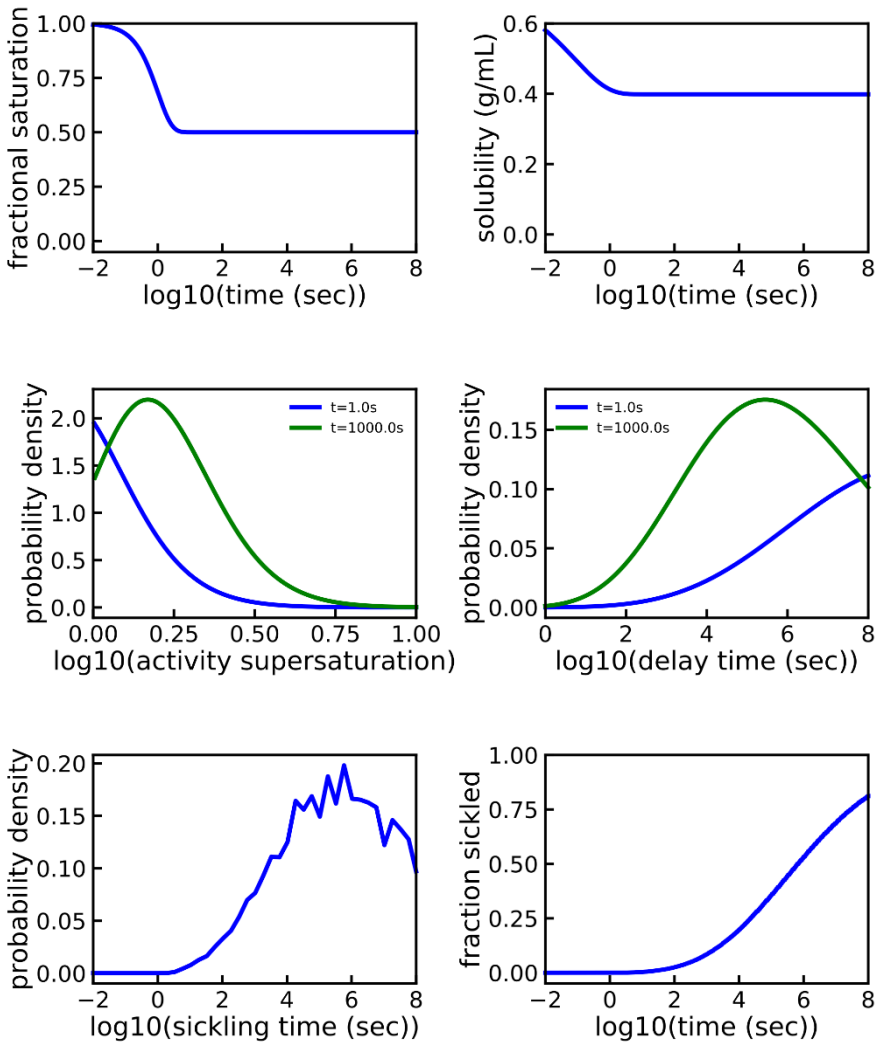

Figure A3: 6 steps in calculation of fraction sickled vs time for 1 sec desaturation to 50% saturated for sickle trait with Lew normal concentration distribution.

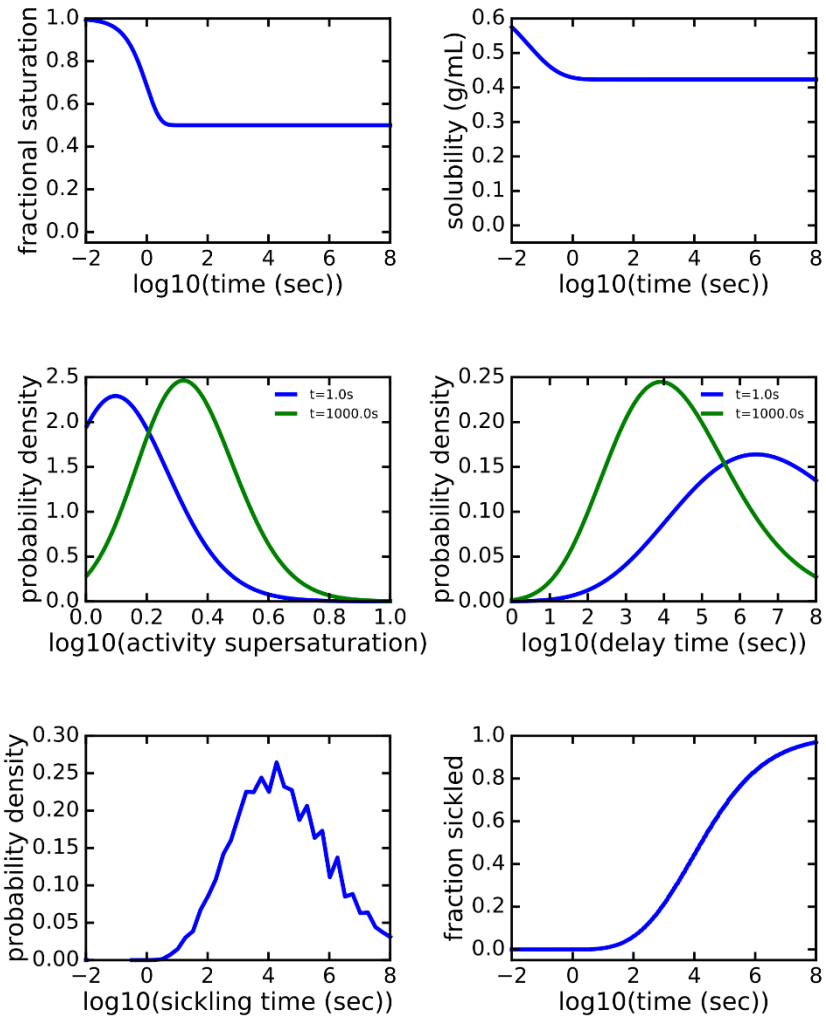

Figure A4: 6 steps in calculation of fraction sickled vs time for 1 sec desaturation to 50% saturated for S/HPFH patient with Lew normal concentration distribution.

Acknowledgements

I am deeply indebted to my many collaborators who have made this thesis possible, especially H. Franklin Bunn, Frank Ferrone, Eric Henry, James Hofrichter, Andrea Mozzarelli, Attila Szabo, and Cristiano Viappiani.

References

1. Dickerson RE & I. G (1983) *Hemoglobin: Structure, function, evolution, and pathology* (Benjamin/Cummings, Menlo Park, CA) p 176.
2. White JG (1974) Ultrastructural features of srythrocyte and hemoglobin sickling. *Arch. Int. Med.* 133(4):545-562.
3. Pauling L, Itano HA, Singer SJ, & Wells IC (1949) Sickle cell anemia, a molecular disease. *Science* 110:543-548.
4. Eaton WA (2003) Linus Pauling and sickle cell disease. *Biophys. Chem.* 100:109-116.
5. Cohen SIA*, et al.* (2011) Nucleated polymerization with secondary pathways. I. Time evolution of the principal moments. *J. Chem. Phys.* 135(6).
6. Cohen SIA, Vendruscolo M, Dobson CM, & Knowles TPJ (2011) Nucleated polymerization with secondary pathways. II. Determination of self-consistent solutions to growth processes described by non-linear master equations. *J. Chem. Phys.* 135(6).
7. Cohen SIA, Vendruscolo M, Dobson CM, & Knowles TPJ (2011) Nucleated polymerization with secondary pathways. III. Equilibrium behavior and oligomer populations. *J. Chem. Phys.* 135(6).
8. Cohen SIA*, et al.* (2013) Proliferation of amyloid-beta 42 aggregates occurs through a secondary nucleation mechanism. *Proc. Natl. Acad. Sci. USA* 110(24):9758-9763.
9. Michaels TCT, Lazell HW, Arosio P, & Knowles TPJ (2015) Dynamics of protein aggregation and oligomer formation governed by secondary nucleation. *J. Chem. Phys.* 143(5).
10. Pauling L (1980) The normal hemoglobins and the hemoglobinopathies - background. *Texas Rep. Biol. Med.* 40:1-7.
11. Sherman IJ (1940) The sickling phenomenon, with special reference to the differentiation of sickle cell anemia from sickle cell trait. *Bull. Johns Hopkins Hospital* 67:309-324.
12. Eaton WA & Hofrichter J (1990) Sickle cell hemoglobin polymerization. *Adv. Prot. Chem.* 40:63-279.
13. Pauling L (1935) The oxygen equilibrium of hemoglobin and its structural interpretation. *Proc. Natl. Acad. Sci. USA* 21:186-191.
14. Pauling L & Coryell CD (1936) The magnetic properties and structure of hemoglobin, oxyhemoglobin and carbonmonoxyhemoglobin. *Proc. Natl. Acad. Sci. USA* 22:210-216.
15. Coryell CD & Pauling L (1940) A structural interpretation of the acidity of groups associated with the hemes of hemoglobin and hemoglobin derivatives. *J. Biol. Chem.* 132(2):769-779.
16. Ingram VM (1957) Gene mutations in human haemoglobin - chemical difference between normal and sickle cell haemoglobin. *Nature* 180(4581):326-328.
17. Muirhead H & Perutz MF (1963) Structure of haemoglobin - a 3-dimensioanl fourier synthesis of reduced human haemoglobin at 5.5 A resolution. *Nature* 199(489):633-&.
18. Perutz MF, Watson HC, Muirhead H, Diamond R, & Bolton W (1964) Structure of haemoglobin - X-ray examination of reduced horse haemoglobin. *Nature* 203(494):687-&.
19. Wishner BC, Ward KB, Lattman EE, & Love WE (1975) Crystal structure of sickle cell deoxyhemoglobin S at 5 A resolution. *J. Mol. Biol.* 98(1):179-194.
20. Dykes GW, Crepeau RH, & Edelstein SJ (1978) Three-dimensional reconstruction of the fibres of sickle cell haemoglobin. *Nature* 272:506-510.
21. Carragher B, Bluemke DA, Gabriel B, Potel MJ, & Josephs R (1988) Structural analysis of polymers of sickle cell hemoglobin 1. sickle hemoglobin fibers. *J. Mol. Biol.* 199(2):315-331.
22. Padlan EA & Love WE (1985) Refined crystal structure of deoxyhemoglobin S. 1. Restrained least squares refinement at 3.0 A resolution. *J. Biol. Chem.* 260(14):8272-8279.
23. Cretegny I & Edelstein SJ (1993) Double strand packing in hemoglobin-S fibers. *J. Mol. Biol.* 230:733-738.
24. Ross PD, Briehl RW, & Minton AP (1978) Temperature dependence of non-ideality in concentrated solutions of hemoglobin. *Biopolymers* 17(9):2285-2288.
25. Sunshine HR, Hofrichter J, Ferrone FA, & Eaton WA (1982) Oxygen binding by sickle-cell hemoglobin polymers. *J. Mol. Biol.* 158(2):251-273.
26. Gill SJ, Benedict RC, Fall L, Spokane R, & Wyman J (1979) Oxygen binding to sickle cell hemoglobin. *J. Mol. Biol.* 130(2):175-189.

27. Monod J, Wyman J, & Changeux JP (1965) On the nature of allosteric transitions: a plausible model. *J. Mol. Biol.* 12(1):88-118.
28. Rivetti C, Mozzarelli A, Rossi GL, Henry ER, & Eaton WA (1993) Oxygen binding by single crystals of hemoglobin. *Biochemistry* 32(11):2888-2906.
29. Henry ER*, et al.* (2015) Experiments on hemoglobin in single crystals and silica gels distinguish among allosteric models. *Biophys. J.* 109(6):1264-1272.
30. Wyman J & Gill SJ (1990) *Binding and Linkage. Functional Chemistry of Biological Macrmolecules* (University Science Books, Mill Valley, CA) p 330.
31. Gill SJ, Spokane R, Benedict RC, Fall K, & Wyman J (1980) Ligand-linked phase equilibria of sickle cell hemoglobin. *J. Mol. Biol.* 140:299-312.
32. Padlan EA & Love WE (1985) Refined crystal structure of deoxyhemoglobin S, 2. molecular interactions in the crystal. *J. Biol. Chem.* 260(14):8280-8291.
33. Henry ER, Bettati S, Hofrichter J, & Eaton WA (2002) A tertiary two-state allosteric model for hemoglobin. *Biophys. Chem.* 98(1-2):149-164.
34. Viappiani C*, et al.* (2004) New insights into allosteric mechanisms from trapping unstable protein conformations in silica gels. *Proc. Natl. Acad. Sci. USA* 101(40):14414-14419.
35. Viappiani C*, et al.* (2014) Experimental basis for a new allosteric model for multisubunit proteins. *Proc. Natl. Acad. Sci. USA* 111(35):12758-12763.
36. Tsai AG, Johnson PC, & Intaglietta M (2003) Oxygen gradients in the microcirculation. *Physiol. Rev.* 83(3):933-963.
37. Fabry ME*, et al.* (1984) Dense cells in sickle cell anemia - the effects of gene interaction. *Blood* 64(5):1042-1046.
38. Lew VL, Raftos JE, Sorette M, Bookchin RM, & Mohandas N (1995) Generation of normal human red-cell volume, hemoglobin content, and membrane area distributions by birth or regulation. *Blood* 86(1):334-341.
39. Kaul DK, Fabry ME, Windisch P, Baez S, & Nagel RL (1983) Erythrocytes in sickle cell anemia are heterogeneous in their rheological and hemodynmaic characteristics. *J. Clin. Invest.* 72(1):22-31.
40. Lew VL & Bookchin RM (2005) Ion transport pathology in the mechanism of sickle cell dehydration. *Phys. Rev.* 85(1):179-200.
41. Cellmer T, Ferrone FA, & Eaton WA (2016) Universality of supersaturation ratio in protein fiber formation. *Nature Struct. Mol. Biol.* 23:459-471.
42. Mozzarelli A, Hofrichter J, & Eaton WA (1987) Delay time of hemoglobin-S polymerization prevents most cells from sickling in vivo. *Science* 237(4814):500-506.
43. Yosmanovich D, Rotter M, Aprelev A, & Ferrone FA (2016) Calibrating sickle cell disease. *J. Mol. Biol.* 428(8):1506-1514.
44. Noguchi CT & Schechter AN (1981) The intracellular polymwerization of sickle hemoglobin and its relevance to sickle-cell disease. *Blood* 58(6):1057-1068.
45. Noguchi CT & Schechter AN (1985) Sickle hemoglobin polymerization in solution and cells. *Ann. Rev. Biophys. Biophys. Chem.* 14:239-263.
46. Steinberg MH, Chui DHK, Dover GJ, Sebastiani P, & Alsultan A (2014) Fetal hemoglobin in sickle cell anemia: a glass half full? *Blood* 123(4):481-485.
47. Bunn HF & Forget BG (1986) *Hemoglobin: Molecular, Genetic and Clinical Aspects* (W. B. Saunders Company) p 690.
48. Brittenham GM, Schechter AN, & Noguchi CT (1985) Hemoglobin S polymerization - primary determinant of the hemolytic and clinical severity of the sickling syndormes. *Blood* 65(1):183-189.
49. Sunshine HR, Hofrichter J, & Eaton WA (1978) Requirements for therapeutic inhibition of sickle hemoglobin gelation. *Nature* 275(5677):238-240.
50. Bohr C, Hasselbalch K, & Krogh A (1904) About a new biological relation of high importance that the blood carbonic acid tension exercises on its oxygen binding. *Skandinavisches Archiv Fur Physiologie* 16:402-412.
51. Coletta M, Hofrichter J, Ferrone FA, & Eaton WA (1982) Kinetics of sickle hemoglobin polymerization in single red-cells. *Nature* 300(5888):194-197.
52. Ilboudo Y*, et al.* (2017) Genome-wide association study of erythrocyte density in sickle cell disease patients. *Blood Cells Molec. Dis.* 65:60-65.
53. Kaul DK, Fabry ME, & Nagel RL (1996) The pathophysiology of vascular obstruction in the sickle syndromes. *Blood Rev.* 10(1):29-44.
54. Aprelev A, Stephenson W, Noh H, Meier M, & Ferrone FA (2012) The Physical foundation of vasoocclusion in sickle cell disease. *Biophys. J,* 103(8):L38-L40.
55. Ferrone FA (2015) The delay time in sickle cell disease after 40 years: A paradigm assessed. *Amer. J. Hematol.* 90(5):438-445.

56. Hebbel RP, Boogaerts MAB, Eaton JW, & Steinberg MH (1980) Erythrocyte adherence to endothelium in sickle cell anemia: a possible determinat of clinical severity. *New Eng. J. Med.* 302(18):992-995.
57. Bunn HF (1997) Mechanisms of disease - Pathogenesis and treatment of sickle cell disease. *New Eng. J. Med.* 337(11):762-769.
58. Kaul DK, Finnegan E, & Barabino GA (2009) Sickle red cell-endotheliumi interactions. *Microcirculation* 16(1):97-111.
59. Eaton WA & Bunn HF (2017) Treatment of sickle cell disease by targeting Hb S polymerization. *Blood* 129(20):2719-2726.
60. Hebbel RP*, et al.* (1980) Abnormal adherenec of sickle erythrocytes to cultured vascular endothelium - a possible mechanism for mico-vascular occulusion in sickle cell disease. *J. Clin. Invest.* 65(1):154-160.
61. Frenette PS & Atweh GF (2007) Sickle cell disease: old discoveries, new concepts, and future promise. *J. Clin. Invest.* 117(4):850-858.
62. Kato GJ, Gladwin MT, & Steinberg MH (2007) Deconstructing sickle cell disease: Reappraisal of the role of hemolysis in the development of clinical subphenotypes. *Blood Rev.* 21(1):37-47.
63. Nath KA & Hebbel RP (2015) Sickle cell disease: renal manifestations and mechanisms. *Nature Rev. Neph.* 11(3):161-171.
64. Telen MJ, Wun T, McCavit T.L. ea, & (2015) Randomized phase 2 study of GMI-1070 in SCD: reduction in time to resolution of vaso-occlusive events and decreased opioid use. *Blood* 125:2656.
65. Ataga KI, Kutlar A, & Kanter J (2017) Crizanlizumab in sickle cell disease. *New Engl. J. Med.* 376(18):1796-1796.
66. Greenberg J, Ohenefrempong K, Halus J, Way C, & Schwartz E (1983) Trial of low doses of aspirin as prophylaxis in sickle cell disease. *J. Peds.* 102(5):781-784.
67. Orringer EP*, et al.* (2001) Purified poloxamer 188 for treatment of acute vaso-occlusive crisis of sickle cell disease - A randomized controlled trial. *J. Amer. Med. Ass.* 286(17):2099-2106.
68. Schnog JB*, et al.* (2001) Low adjusted-dose acenocoumarol therapy in sickle cell disease: A pilot study. *Amer. J. Hrmatol.* 68(3):179-183.
69. Ataga KI*, et al.* (2011) Improvements in haemolysis and indicators of erythrocyte survival do not correlate with acute vaso-occlusive crises in patients with sickle cell disease: a phase III randomized, placebo-controlled, double-blind study of the gardos channel blocker senicapoc (ICA-17043). *Brit. J. Hematol.* 153(1):92-104.
70. Gladwin MT*, et al.* (2011) Nitric Oxide for Inhalation in the Acute Treatment of Sickle Cell Pain Crisis A Randomized Controlled Trial. *J. Amer. Med. Ass.* 305(9):893-902.
71. Machado RF*, et al.* (2011) Hospitalization for pain in patients with sickle cell disease treated with sildenafil for elevated TRV and low exercise capacity. *Blood* 118(4):855-864.
72. Desai PC*, et al.* (2013) A pilot study of eptifibatide for treatment of acute pain episodes in sickle cell disease. *Thromb. Res.* 132(3):341-345.
73. Heeney MM*, et al.* (2016) A Multinational Trial of Prasugrel for Sickle Cell Vaso-Occlusive Events. *New Engll. J. Med.* 374(7):625-635.
74. Eaton WA, Hofrichter J, & Ross PD (1976) Delay time of gelation - possible determinant of clinical severity in sickle-cell disease. *Blood* 47(4):621-627.
75. Bunn HF (1997) Mechanisms of disease - Pathogenesis and treatment of sickle cell disease. *N. Engl. J. Med.* 337:762-769.
76. Eaton WA & Hofrichter J (1987) Hemoglobin-S gelation and sickle-cell disease. *Blood* 70(5):1245-1266.
77. Benesch RE, Kwong S, Benesch R, & Edalji R (1977) Location and bond type of intermolecular contacts in polymerization of hemoglobin S. *Nature* 269(5631):772-775.
78. Nagel RL*, et al.* (1980) Beta chain contact sites in the hemoglobin S polymer. *Nature* 283(5750):832-834.
79. Shan YB*, et al.* (2011) How does a drug molecule find its target binding site? *J. Amer. Chem. Soc.* 133(24):9181-9183.
80. Charache S*, et al.* (1996) Hydroxyurea and sickle cell anemia - Clinical utility of a myelosuppressive "switching" agent. *Medicine* 75(6):300-326.
81. Goldberg MA*, et al.* (1990) Treatment of sickle cell anemia with hydroixyurea and erythropieotin. *New Eng. J. Med.* 323(6):366-372.
82. Bauer DE, Kamran SC, & Orkin SH (2012) Reawakening fetal hemoglobin: prospects for new therapies for the beta-globin disorders. *Blood* 120(15):2945-2953.
83. Sankaran VG*, et al.* (2008) Human fetal hemoglobin expression is regulated by the developmental stage-specific repressor BCL11A. *Science* 322(5909):1839-1842.

84. Xu J*, et al.* (2011) Correction of sickle cell disease in adult mice by interference with fetal hemoglobin silencing. *Science* 334(6058):993-996.
85. Eaton WA & Hofrichter J (1995) The biophysics of sickle cell hydroxyurea therapy. *Science* 268:1142-1143.
86. Bunn HF & McDonough M (1974) Asymmterical hemoglobin hybrids - approach to study of subunit interactions. *Biochemistry* 13(5):988-993.
87. Goldberg MA, Husson MA, & Bunn HF (1977) Participation of hemoglbins A and F in polymerization of sickle cell hemoglobin. *J. Biol. Chem.* 252(10):3414-3421.
88. Minton AP (1977) Non-ideality and thermodynamics of sickle cell hemoglobin gelation. *J. Mol. Biol.* 110(1):89-103.
89. Benesch RE, Edalji R, Benesch R, & Kwong S (1980) Solubilization of hemoglobin S by other hemoglobins. *Proc. Natl. Acad. Sci. USA* 77(9):5130-5134.
90. Ross PD & Minton AP (1977) Analysis of non-ideal behavior in concentrated hemoglobin solutions. *J. Mol. Biol.* 112(3):437-452.
91. Sunshine HR, Hofrichter J, & Eaton WA (1979) Gelation of sickle-cell hemoglobin in mixtures with normal adult and fetal hemoglobins. *J. Mol. Biol.* 133(4):435-467.
92. Ferrone FA, Hofrichter J, & Eaton WA (1985) Kinetics of sickle hemoglobin polymerization 2. A double nucleation mechanism. *J. Mol. Biol.* 183(4):611-631.
93. Eaton WA, Henry ER, Hofrichter J, & Mozzarelli A (1999) Is cooperative oxygen binding by hemoglobin really understood? *Nature Struct. Biol.* 6(4):351-358.
94. Beutler E (1961) Effect of methemoglobin formation in sickle cell disease. *J. Clin. Invest.* 40(10):1856-&.
95. Beutler E (1975) Effect of carbon monoxide on red cell life span in sickle cell diseaes. *Blood* 46(2):253-259.
96. Abraham DJ*, et al.* (1991) Vanillin, a potential agent for the treatment of sickle cell anemia. *Blood* 77(6):1334-1341.
97. Kato GJ (2016) New insights into sickle cell disease: mechanisms and investigational therapies. *Curr. Opin. Hemat.* 23(3):224-232.
98. Benesch R & Benesch RE (1969) Intracellular organic phosphates as regulators of oxygen release by haemoglobin. *Nature* 221(5181):618-&.
99. Bunn HF & Jandl JH (1970) Control of hemoglobin function within the red cell. *N. Eng, J. Med.* 282(25):1414-&.
100. Bunn HF (1981) Evolution of mammalian hemoglobin function. *Blood* 58(2):189-197.
101. Perutz MF (1970) The Bohr effect and combination with organic phosphates. *Nature* 228(5273):734-739.
102. Bunn HF & Briehl RW (1970) Interaction of 2,3-diphosphoglycerate with various human hemoglobins. *J. Clin. Invest.* 49(6):1088-&.
103. Beutler E, Paniker NV, & West C (1971) The effect of 2,3-DPG on the sickling phenomenon. *Blood* 37:184–186.
104. Poillon WN & Kim BC (1990) 2,3-Diphosphoglycerate and intracelular pH as interdependent determinants of the physiological solubility of deoxyhemoglobin S. *Blood* 76(5):1028-1036.
105. Hofrichter J, Ross PD, & Eaton WA (1976) Supersaturation in sickle cell hemoglobin solutions. *Proc. Natl. Acad. Sci. USA* 73:3034-3039.
106. Poillon WN, Kim BC, Labotka RJ, Hicks CU, & Kark JA (1995) Antisickling effects of 2,3-diphosphoglycerate depeletion. *Blood* 85(11):3289-3296.
107. Cohen-Solal M*, et al.* (1998) A new sickle cell disease phenotype associating Hb S trait, severe pyruvate kinase deficiency (PK Conakry), and an alpha 2 globin gene variant (Hb Conakry). *Brit. J. Hematol.* 103(4):950-956.
108. Alli N*, et al.* (2008) Sickle cell disease in a carrier with pyruvate kinase deficiency. *Hematol.* 13(6):369-372.
109. Rose ZB & Liebowitz J (1970) 2,3-Diphosphosphoglycerate phosphatase - general properties and inactivation by anions. *J. Biol. Chem.* 245(12):3232-3241.
110. Rose ZB (1976) Procedure for decreasing level of 2,3-biphosphoflycerate in red cells in vitro. *Biochem. Biophys. Res. Comm.* 73(4):1011-1017.
111. Hofrichter J, Ross PD, & Eaton WA (1974) Kinetics and mechanism of deoxyhemoglobin-S gelation - new approach to understanding sickle-cell disease. *Proc. Natl. Acad. Sci. USA* 71(12):4864-4868.
112. Ponder E (1949) The tonicity-volume relations for sytems containing human red cells and the chlorides of monovalent cations. *J. Gen. Physiol.* 32:391–398.
113. Rosa RM*, et al.* (1980) A study of hyponatremia in the prevention and treatment of sickle cell crsis. *New Engl. J. Med.* 303(20):1138-1143.

114. Das N*, et al.* (2015) Intestine-specific Disruption of Hypoxia-inducible Factor (HIF)-2 alpha Improves Anemia in Sickle Cell Disease. *J. Biol. Chem.* 290(39):23523-23527.
115. Castro O, Poillon WN, Finke H, Massac E, & Kim BC (1994)
Improvement of sickle cell anemia by iron limited erythropoiesis. *Amer. J. Hematol.* 47(2):74-81.
116. Stocker JW*, et al.* (2003) ICA-17043, a novel Gardos channel blocker, prevents sickled red blood cell dehydration in vitro and in vivo in SAD mice. *Blood* 101(6):2412-2418.
117. Ataga KI*, et al.* (2008) Efficacy and safety of the Gardos channel blocker, senicapoc (ICA-17043), in patients with sickle cell anemia. *Blood* 111(8):3991-3997.
118. Ataga KI & Stocker J (2015) The trials and hopes for drug development in sickle cell disease. *Brit. J. Hematol.* 170(6):768-780.
119. Clark MR, Mohandas N, & Shohet SB (1982) Hydration of sickle cells using the sodium ionophore monensin - a model for therapy. *J. Clin. Invest.* 70(5):1074-1080.
120. Li Q*, et al.* (2017) Kinetic assay shows that increasing red cell volume could be a treatment for sickle cell diseaes. *Proc. Natl. Acad. Sci. USA* early edition online.
121. Telen MJ (2016) Beyond hydroxyurea: new and old drugs in the pipeline for sickle cell disease. *Blood* 127(7):810-819.
122. Wambebe C*, et al.* (2001) Double-blind, placebo-controlled, randomised cross-over clinical trial of NIPRISAN (R) in patients with sSickle cell disorder. *Phytomedicine* 8(4):252-261.
123. Wambebe CO*, et al.* (2001) Efficacy of niprisan in the prophylactic management of patients with sickle cell disease. *Curr. Ther. Res,-Clin. Expt.* 62(1):26-34.
124. Iyamu EW, Turner EA, & Asakura T (2002) In vitro effects of NIPRISAN (Nix-0699): a naturally occurring, potent antisickling agent. *Brit. J. Haematol.* 118(1):337-343.
125. Iyamu EW, Turner EA, & Asakura T (2003) Niprisan (Nix-0699) improves the survival rates of transgenic sickle cell mice under acute severe hypoxic conditions. *Brit. J. Haematol.* 122(6):1001-1008.
126. Swift R*, et al.* (SCD-101: A new anti-sickling drug reduces pain and fatigue and improves red blood cell shape in peripheral blood of patients with sickle cell disease. *Blood* 128(22):121.
127. Abdulmalik O*, et al.* (2005) 5-hydroxymethyl-2-furfural modifies intracellular sickle haemoglobin and inhibits sickling of red blood cells. *Brit. J. Haematol.* 128(4):552-561.
128. van Beers EJ*, et al.* (2014) Imaging flow cytometry for automated detection of hypoxia-induced erythrocyte shape change in sickle cell disease. *Amer. J. Hematol.* 89(6):598-603.
129. Oder E, Safo MK, Abdulmalik O, & Kato GJ (2016) New developments in anti-sickling agents: can drugs directly prevent the polymerization of sickle haemoglobin in vivo? *Brit. J. Haematol.* 175:24-30.
130. Metcalf B*, et al.* (2017) Discovery of GBT440, an Orally Bioavailable R-State Stabilizer of Sickle Cell Hemoglobin. *ACS Med. Chem. Lett.* 8(3):321-326.
131. Lehrer-Graiwer J*, et al.* (2015) GBT440, a potent anti-sickling hemoglobin modifier reduces hemolysis, improves anemia and nearly eliminates sickle cells in peripheral blood of patients with sickle cell disease. *Blood* 126:542.
132. Lehrer-Graiwer J*, et al.* (2016) Long-term dosing in sickle cell disease subjects with GBT440, a novel HbS polymerization inhibitor. *Blood* 128,:2488.
133. Hsieh MM, Fitzhugh CD, & Tisdale JF (2011) Allogeneic hematopoietic stem cell transplantation for sickle cell disease: the time is now. *Blood* 118(5):1197-1207.
134. Robinson TM & Fuchs EJ (2016) Allogeneic stem cell transplantation for sickle cell disease. *Curr. Opin. Hematol.* 23(6):524-529.
135. Lettre G & Bauer DE (2016) Fetal haemoglobin in sickle-cell disease: from genetic epidemiology to new therapeutic strategies. *Lancet* 387(10037):2554-2564.
136. McGann PT, Hernandez AG, & Ware RE (2017) Sickle cell anemia in sub-Saharan Africa: advancing the clinical paradigm through partnerships and research. *Blood* 129(2):155-161.
137. Platt OS*, et al.* (1984) Hydroxyurea enhances fetal hemoglobin production in sickle cell anemia. *J. Clin. Invest.* 74(2):652-656.
138. Charache S*, et al.* (1995) Effect of hydroxyurea on the frequency of painful crises in sickle cell anemia. *N. Engl. J. Med.* 332:1317-1322.
139. Ware RE (2015) Optimizing hydroxyurea therapy for sickle cell anemia. *Hematology*:436-443.
140. Platt OS*, et al.* (1984) Hydroxyurea enhances fetal hemoglobin production in sickle-cell-anemia. *J. Clin. Invest.* 74(2):652-656.
141. Bridges KR*, et al.* (1996) A multiparameter analysis of sickle erythrocytes in patients undergoing hydroxyurea therapy. *Blood* 88(12):4701-4710.
142. Lanzkron S, Haywood C, Segal JB, & Dover GJ (2006) Hospitalization rates and costs of care of patients with sickle-cell anemia in the State of Maryland in the era of hydroxyurea. *Am. J. Hematol.* 81(12):927-932.

143. Steinberg MH*, et al.* (2010) The risks and benefits of long-term use of hydroxyurea in sickle cell anemia: A 17.5 year follow-up. *Amer. J. Hematol.* 85(6):403-408.
144. Fitzhugh CD*, et al.* (2015) Hydroxyurea-increased fetal Hemoglobin is associated with less organ damage and longer survival in adults with sickle cell anemia. *Plos One* 10(11).
145. Brugnara C, Bunn HF, & Tosteson DC (1986) Regulation of erythrocyte cation and water content in sickle cell anemia. *Science* 232(4748):388-390.
146. Zarkowsky HS & Hochmuth RM (1975) Sickling times of individual erythrocytes at zero pO2. *J. Clin. Invest.* 56(4):1023-1034.
147. Rotter M, Yosmanovich D, Briehl RW, Kwong S, & Ferrone FA (2011) Nucleation of sickle hemoglobin mixed with hemoglobin A: experimental and theoretical studies of hybrid-forming mixtures. *Biophys. J.* 101(11):2790-2797.
148. Christoph GW, Hofrichter J, & Eaton WA (2005) Understanding the shape of sickled red cells. *Biophys. J.* 88(2):1371-1376.
149. Bunn HF*, et al.* (1982) Molecular and cellular pathogenesis of hemoglobin SC disease. *Proc. Natl. Acad. Sci. USA* 79(23):7527-7531.
150. Nagel RL, Fabry ME, & Steinberg MH (2003) The paradox of hemoglobin SC disease. *Blood Rev.* 17(3):167-178.
151. Hofrichter J (1979) Ligand binding and the gelation of sickle cell hemoglobin. *J. Mol. Biol.* 128(3):335-&.
152. Ferrone FA, Hofrichter J, & Eaton WA (1985) Kinetics of sickle hemoglobin polymerization; I. Studies using temperature jump and laser photolysis techniques. *J. Mol. Biol.* 183:591-610.
153. Rotter M, Aprelev A, Adachi K, & Ferrone FA (2005) Molecular crowding limits the role of fetal hemoglobin in therapy for sickle cell disease. *J. Mol. Biol.* 347(5):1015-1023.